ARECIBO PULSAR SURVEY USING ALFA. IV. MOCK SPECTROMETER DATA ANALYSIS, SURVEY SENSITIVITY, AND THE DISCOVERY OF 40 PULSARS

P. Lazarus[1], A. Brazier[2,3], J. W. T. Hessels[4,5], C. Karako-Argaman[6], V. M. Kaspi[6], R. Lynch[6,7], E. Madsen[6], C. Patel[6], S. M. Ransom[8], P. Scholz[6], J. Swiggum[7], W. W. Zhu[1], B. Allen[9,10,11], S. Bogdanov[12], F. Camilo[12], F. Cardoso[7], S. Chatterjee[2], J. M. Cordes[2], F. Crawford[13], J. S. Deneva[14], R. Ferdman[6], P. C. C. Freire[1], F. A. Jenet[15], B. Knispel[9], K. J. Lee[16], J. van Leeuwen[4,5], D. R. Lorimer[7], A. G. Lyne[17], M. A. McLaughlin[7], X. Siemens[11], L. G. Spitler[1], I. H. Stairs[18], K. Stovall[19], and A. Venkataraman[20]

[1] Max-Planck-Institut für Radioastronomie, Auf dem Hügel 69, D-53121 Bonn, Germany; plazarus@mpifr-bonn.mpg.de
[2] Dept. of Astronomy, Cornell Univ., Ithaca, NY 14853, USA
[3] Center for Advanced Computing, Cornell Univ., Ithaca, NY 14853, USA
[4] ASTRON, The Netherlands Institute for Radio Astronomy, Postbus 2, 7990 AA, Dwingeloo, The Netherlands
[5] Anton Pannekoek Institute for Astronomy, Univ. of Amsterdam, Science Park 904, 1098 XH Amsterdam, The Netherlands
[6] Dept. of Physics, McGill Univ., Montreal, QC H3A 2T8, Canada
[7] Dept. of Physics, West Virginia Univ., Morgantown, WV 26506, USA
[8] NRAO, Charlottesville, VA 22903, USA
[9] Max-Planck-Institut für Gravitationsphysik, D-30167 Hannover, Germany
[10] Leibniz Universität Hannover, D-30167 Hannover, Germany
[11] Physics Dept., Univ. of Wisconsin—Milwaukee, Milwaukee WI 53211, USA
[12] Columbia Astrophysics Laboratory, Columbia Univ., New York, NY 10027, USA
[13] Dept. of Physics and Astronomy, Franklin and Marshall College, Lancaster, PA 17604-3003, USA
[14] National Research Council, resident at the Naval Research Laboratory, Washington, DC 20375, USA
[15] Center for Gravitational Wave Astronomy, Univ. of Texas—Brownsville, Brownsville, TX 78520, USA
[16] Kavli Institute for Astronomy and Astrophysics, Peking Univ., Beijing 100871, P.R. China
[17] Jodrell Bank Centre for Astrophysics, Univ. of Manchester, Manchester, M13 9PL, UK
[18] Dept. of Physics and Astronomy, Univ. of British Columbia, Vancouver, BC V6T 1Z1, Canada
[19] Dept. of Physics and Astronomy, Univ. of New Mexico, NM 87131, USA
[20] Arecibo Observatory, HC3 Box 53995, Arecibo, PR 00612, USA

ABSTRACT

The on-going Arecibo Pulsar-ALFA (PALFA) survey began in 2004 and is searching for radio pulsars in the Galactic plane at 1.4 GHz. Here we present a comprehensive description of one of its main data reduction pipelines that is based on the PRESTO software and includes new interference-excision algorithms and candidate selection heuristics. This pipeline has been used to discover 40 pulsars, bringing the survey's discovery total to 144 pulsars. Of the new discoveries, eight are millisecond pulsars (MSPs; $P < 10$ ms) and one is a Fast Radio Burst (FRB). This pipeline has also re-detected 188 previously known pulsars, 60 of them previously discovered by the other PALFA pipelines. We present a novel method for determining the survey sensitivity that accurately takes into account the effects of interference and red noise: we inject synthetic pulsar signals with various parameters into real survey observations and then attempt to recover them with our pipeline. We find that the PALFA survey achieves the sensitivity to MSPs predicted by theoretical models but suffers a degradation for $P \gtrsim 100$ ms that gradually becomes up to ~10 times worse for $P > 4$ s at DM < 150 pc cm^{-3}. We estimate $33 \pm 3\%$ of the slower pulsars are missed, largely due to red noise. A population synthesis analysis using the sensitivity limits we measured suggests the PALFA survey should have found 224 ± 16 un-recycled pulsars in the data set analyzed, in agreement with the 241 actually detected. The reduced sensitivity could have implications on estimates of the number of long-period pulsars in the Galaxy.

Key words: methods: data analysis – pulsars: general

1. INTRODUCTION

Pulsars are rapidly rotating, highly magnetized neutron stars, the remnants of massive stars after their death in supernova explosions. They are extremely valuable astronomical tools with many physical applications that have been used to, for example, constrain the equation of state of ultra-dense matter (e.g., Hessels et al. 2006; Demorest et al. 2010), test relativistic gravity (e.g., Kramer et al. 2006b; Antoniadis et al. 2013), probe plasma physics within the magnetosphere (e.g., Hankins et al. 2003; Kramer et al. 2006a; Lyne et al. 2010; Hermsen et al. 2013), and gain a better understanding of the complete radio pulsar population (e.g., Faucher-Giguère & Kaspi 2006). Certain individual pulsar systems are especially well suited to studying these areas of astrophysics, and thus continued pulsar

surveys to find these rare objects remain an important step of scientific discovery in the field.

Radio pulsars are found primarily in non-targeted, wide-area surveys such as the Pulsar-ALFA (PALFA) survey at 1.4 GHz, which began in 2004 (Cordes et al. 2006). PALFA observations use the 7-beam Arecibo L-band Feed Array (ALFA) receiver of the Arecibo Observatory William E. Gordon 305 m Telescope and focus on the Galactic plane ($|b| < 5°$) in the two regions visible with Arecibo, namely the "inner Galaxy" region ($32° \lesssim l \lesssim 77°$), and the "outer Galaxy" region ($168° \lesssim l \lesssim 214°$).

For the first 5 years, PALFA survey observations were made using the Wideband Arecibo Pulsar Processor (WAPP), a 3-level auto-correlation spectrometer with 100 MHz of

bandwidth (Dowd et al. 2000). Since 2009, the Mock spectrometer,[21] a 16 bit poly-phase filterbank, has replaced the WAPP spectrometer as the data-recorder of the PALFA survey. The Mock spectrometer records two critically sampled, overlapping 172 MHz bands that fully cover the 322 MHz ALFA band. The increased bandwidth, poly-phase filterbank design, and increased bit-depth of the Mock spectrometer have increased the sensitivity and robustness to interference of the PALFA survey. For this reason, we are re-observing regions of the sky previously observed with the WAPP spectrometers.

The PALFA consortium currently employs two independent full-resolution data analysis pipelines. The Einstein@Home-based pipeline (E@H)[22] has already been described by Allen et al. (2013): this pipeline derives its computational power by aggregating the spare cycles of a global network of PCs and mobile devices using the BOINC platform,[23] and is also searching data from the PALFA survey for pulsars. In this work we describe the pipeline based on the PRESTO suite of pulsar search programs[24] (Ransom 2001). In addition to these pipelines, we also employ a reduced-resolution "Quicklook" pipeline, which is run on-site at Arecibo shortly after observing sessions are complete and which enables a more rapid discovery and confirmation of strong pulsars (Stovall 2013).

As of 2015 March, there have been 144 pulsars discovered in WAPP and Mock spectrometer observations with the various PALFA data analysis pipelines. This is already a sizable increase on the previously known sample[25] of 169 Galactic radio pulsars in the survey region out to $|b| < 2°$, the Galactic latitude range we have focused on with the Mock spectrometers.

The relatively high observing frequency and unparalleled sensitivity of Arecibo, coupled with the high time and frequency resolution of PALFA ($\tau_{samp} \simeq 65.5\,\mu s$ and $\Delta f_{chan} \simeq 336\,kHz$, respectively) make it particularly well suited for detecting millisecond pulsars (MSPs) deep in the plane of the Galaxy, such as the distant MSPs reported by Crawford et al. (2012) and Scholz et al. (2015), the highly eccentric MSP PSR J1903+0327 (Champion et al. 2008), and faint, young pulsars (e.g., Hessels et al. 2008). The huge instantaneous sensitivity of Arecibo enables short integration times, which has been helpful in detecting relativistic binaries (e.g., PSR J1906+0746; Lorimer et al. 2006b) by reducing the deleterious effect of time-varying Doppler shifts of binary pulsars. The PALFA survey has also proven successful at detecting transient astronomical signals. For example, the survey has led to the discovery of several Rotating Radio Transient pulsars (RRATs; Deneva et al. 2009), as well as FRB 121102, the first Fast Radio Burst (FRB) detected with a telescope other than the Parkes Radio Telescope (Spitler et al. 2014).

While PALFA is the most sensitive large-scale survey for radio pulsars ever conducted, it is not the only on-going radio pulsar survey. Other major surveys are the HTRU-S (Keith et al. 2010), HTRU-N (Barr et al. 2013), and SPAN512 (Desvignes et al. 2013) surveys at ~1.4 GHz, the GBNCC (Stovall et al. 2014) and AO327 drift (Deneva et al. 2013)

surveys at ~350 MHz, and the LOFAR surveys (Coenen et al. 2014) at ~150 MHz.

The underlying distributions of the pulsar population can be estimated using simulation techniques (e.g., Faucher-Giguère & Kaspi 2006; Lorimer et al. 2006a; Bates et al. 2014). The large sample of pulsars found in non-targeted surveys are essential for these simulations. However, for population analyses to be done accurately, the selection biases of each survey must be taken into account. While the sensitivity of pulsar search algorithms is reasonably well understood, the effect of radio frequency interference (RFI) on pulsar detectability has not been previously studied in detail.

This paper reports on the current state of PALFA's primary search pipeline, its discoveries, and its sensitivity. The rest of the article is organized as follows: the observing set-up is summarized in Section 2. The details of the PALFA PRESTO-based pipeline are described in Section 3. Section 4 reports basic parameters of the pulsars found with the pipeline, and Section 5 details how the survey sensitivity is determined, including a technique involving injecting synthetic pulsars into the data. These accurate sensitivity limits are used to improve upon population synthesis analyses in Section 6. The broader implications of the accurate determination of the survey sensitivity are presented in Section 7 before the paper is summarized in Section 8.

2. OBSERVATIONS

The PALFA survey observations have been restricted to the two regions of the Galactic plane ($|b| < 5°$) visible from the Arecibo observatory, the inner Galaxy ($32° \lesssim l \lesssim 77°$), and the outer Galaxy ($168° \lesssim l \lesssim 214°$). Integration times are 268 s and 180 s for inner and outer Galaxy observations, respectively.

To optimize the use of telescope resources, the PALFA survey operates in tandem with other compatible projects using the ALFA 7-beam receiver. In particular, we have reciprocal data-sharing agreements with collaborations that search for galaxies in the optically obscured ("zone of avoidance") directions through the Milky Way (Henning et al. 2010) and recombination-line studies of ionized gas in the Milky Way (Liu et al. 2013). The PALFA project leads inner Galaxy observing sessions, whereas our partners lead outer Galaxy sessions.

For the inner Galaxy region, the pointing strategy has prioritized observations of the $|b| < 2°$ region before moving on to the Galactic plane at larger Galactic latitudes. Our pointing grid densely samples patches of sky out to the ALFA beam FWHM by interleaving three ALFA pointings (see Cordes et al. 2006, for more details). In contrast, our commensal partners have focused outer Galaxy observations in order to densely sample particular Galactic longitude/latitude ranges. A sky map showing the pointing positions observed with the Mock spectrometers can be found in Figure 1.

Observations conducted with ALFA have a bandwidth of 322 MHz centered at 1375 MHz. Each of the seven ALFA beams is split into two overlapping 172 MHz sub-bands and processed independently by the Mock spectrometers.[26] The sub-bands are divided into 512 channels. The data are recorded with a time resolution of ~65.5 μs. The observing parameters

---

[21] http://www.naic.edu/~astro/mock.shtml
[22] http://einstein.phys.uwm.edu/
[23] http://boinc.berkeley.edu/
[24] http://www.cv.nrao.edu/~sransom/presto/
[25] As listed in the ATNF Pulsar Catalogue: http://www.atnf.csiro.au/research/pulsar/psrcat (Manchester et al. 2005).

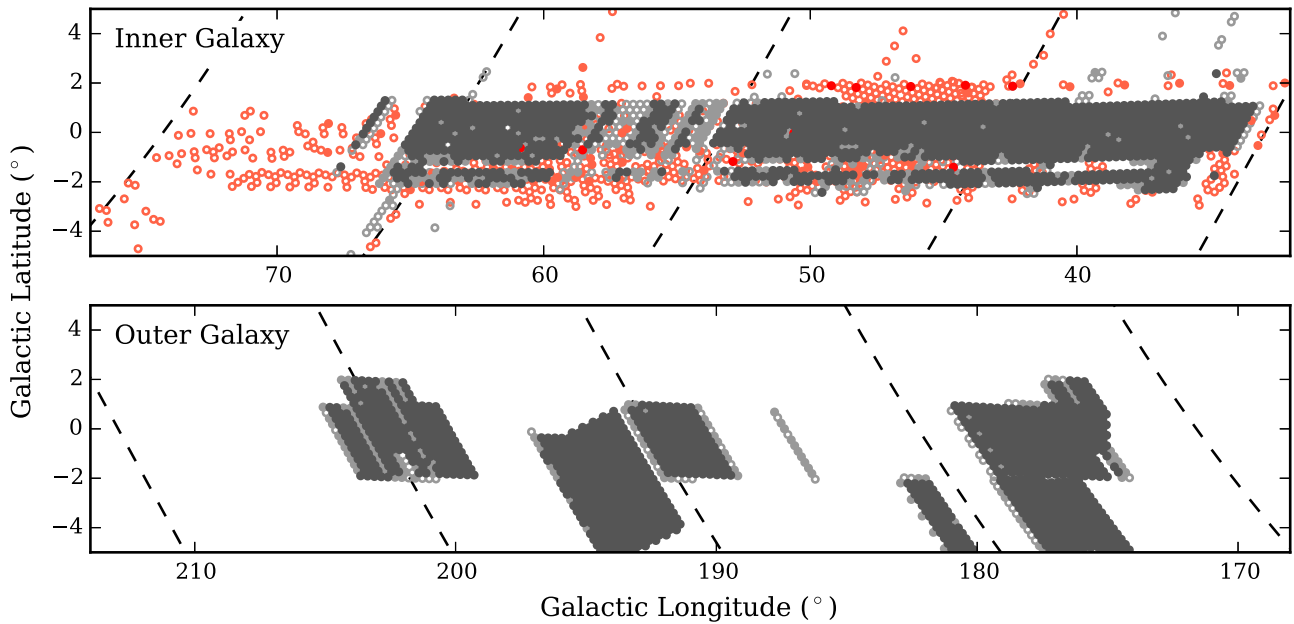[26] http://www.naic.edu/~astro/mock.shtml

Figure 1. Sky map showing the locations of PALFA observations with the Mock spectrometers, which began in 2009, for the inner and outer Galaxy regions. Observations up until 2014 December are included. Each position plotted represents the center of the 3-pointing set required to densely sample the area. Positions that have been only sparsely observed (i.e., 1 of 3 pointing positions observed) are indicated with un-filled circles. Positions with 2 of 3 pointings observed are indicated with a light-colored filled circle. Positions that have been densely observed (i.e., all 3 pointing positions observed) are indicated with dark-colored filled circles. Red indicates observations made prior to adjusting our pointing grid at the request of our commensal partners. As a result, some of the sky area covered in early Mock observations has not been re-observed using the Mocks and the current commensal pointing grid.

Table 1
PALFA Mock Spectrometer Observing Set-up Parameters

Parameter	Value
General	
Sample Time, τ_{samp} (μs)	65.476
Integration Time[a], t_{obs} (s)	268 (Inner Galaxy, $32° \lesssim l \lesssim 77°$)
	180 (Anti-center, $168° \lesssim l \lesssim 214°$)
High Sub-band	
Number of Channels	512
Low Frequency (MHz)	1364.290
High Frequency (MHz)	1536.016
Low Sub-band	
Number of Channels	512
Low Frequency (MHz)	1214.290
High Frequency (MHz)	1386.016
Merged Band	
Number of Channels	960
Low Frequency (MHz)	1214.290
Center Frequency (MHz)	1375.489
High Frequency (MHz)	1536.688
Bandwidth, Δf (MHz)	322.398
Channel Bandwidth, Δf_{chan} (kHz)	335.831

Note.
[a] This is the integration time remaining after the $\sim$5–10 s calibration diode signal is removed (see Section 3.2).

are summarized in Table 1. The data are recorded to disk in 16 bit search-mode PSRFITS format (Hotan et al. 2004).

PALFA survey data have been recorded with the Mock spectrometers since 2009. However, note that in 2011 our pointing grid was altered slightly to accommodate our commensal partners. This required some sky positions to be re-observed. Prior to 2009, survey observations were recorded with the WAPPs (see Dowd et al. 2000; Cordes et al. 2006). The two data recording systems were run in parallel during 2009 to check the consistency and quality of the Mock spectrometer data.

An unpulsed calibration diode is fired during the first (or sometimes last) 5–10 s of our integration. While this is primarily used by our partners, we have found the diode signals useful in calibrating observations for our sensitivity analysis (see Section 5.4). The calibration signal is removed from the data prior to searching (see Section 3.2).

The original 16 bit Mock data files are compressed to have 4 bits per sample. These smaller data files are more efficient to ship and analyze thanks to reduced disk-space requirements. The 4 bit data files utilize the *scales* and *offsets* fields of the PSRFITS format to retain information about the bandpass shape despite the reduced dynamic range. The scales and offsets are computed and stored for every 1 s sub-integration. This reduction of bit-depth results in a total loss of only a few percent in the signal-to-noise ratio (S/N) of pulsar signals (see e.g., Kouwenhoven & Voûte 2001).

The converted 4-bit PSRFITS data files are copied to hard disks, and couriered from Arecibo to Cornell University where they are archived at the Cornell University Center for Advanced Computing (CAC). Metadata about each observation, parsed from the telescope logs and the file headers, are stored in a dedicated database.

As of 2014 November, a total of 87,689 beams of Mock spectrometer data have been archived. The break-down of observed, archived and analyzed sky positions for the two survey regions is shown in Table 2.

Table 2
Breakdown of PALFA Mock Spectrometer Data

	No. Beams[a]	No. Unique Sky Positions	Sky Coverage (sq. deg.)	Completeness[b], $|b| < 2°$ (%)	Completeness[b], $|b| < 5°$ (%)
Inner Galaxy ($32° \lesssim l \lesssim 77°$)					
Observed	40705	38479	94	69	32
Archived	35030	33243	81	60	27
Analyzed	33888	32499	80	58	27
Anti-center ($168° \lesssim l \lesssim 214°$)					
Observed	60305	26194	64	30	18
Archived	52659	21990	54	23	15
Analyzed	51445	21899	54	23	15

Notes. Including observations up until 2014 December.
[a] There are 7 beams per pointing.
[b] The completeness percentages are relative to the number of pointings we aim to eventually cover with the Mock spectrometers.

PALFA observations more than one year old are publicly available. Small quantities of data can be requested via the web.[27] Access to larger amounts of data is also possible, but must be coordinated with the collaboration because of the logistics involved.

Additional details about the data management logistics and data preparation are in Sections 3.1 and 3.2.

3. PULSAR AND TRANSIENT SEARCH PIPELINE

The PRESTO-based pipeline has been used to search PALFA observations taken with the Mock spectrometers since mid-2011 for radio pulsars and transients. All processing is done using the Guillimin supercomputer of McGill University's High Performance Computing center.[28]

While the pipeline described here was designed specifically for the PALFA survey, it is sufficiently flexible to serve as a base for the data reduction pipeline of other surveys. For example, the SPAN512 survey being undertaken at the Nançay Radio Telescope uses a version of the PALFA PRESTO pipeline described here tuned to their specific needs (Desvignes et al. 2013). The PALFA pipeline source code is publicly available online.[29]

Since the analysis began with the pipeline, there have been several major improvements, primarily focusing on ameliorating its robustness in the presence of RFI (Section 3.4), as well as post-processing algorithms for identifying the best pulsar candidates (Section 3.5). The PALFA consortium is constantly monitoring the performance of the pipeline and the RFI environment at Arecibo (as described later, RFI is one of the major challenges), and looking for ways to further improve the analysis. Here we report on the state of the software as of early-2015.

The pipeline overview presented here is grouped into logical components. In Section 3.1 we outline the significant data tracking and processing logistics required to automate the analysis. In Section 3.2 we detail the data file preparation required before searching an observation. In Section 3.3 we describe the techniques used to search for periodic and impulsive pulsar signals. In Section 3.4 we summarize the various complementary stages of RFI identification and mitigation. Finally, in Sections 3.5 and 3.6 we outline the tools used to help select and view pulsar candidates, as well as other on-line collaborative facilities used by the PALFA consortium.

Figure 2 shows a flowchart summarizing the stages of the pipeline.

3.1. Logistics

The PALFA search pipeline is designed to be almost entirely automated. This includes the logistics of data management required to maintain the analysis of ∼1000 beams on the Guillimin supercomputer at any given time. This is accomplished with a *job-tracker* database that maintains the status of processes that are downloading raw data, reducing data, and uploading results.

The pipeline is configured to continually request and download raw data that have not been processed and delete the local copies of files that have been successfully analyzed. Data files are copied to McGill via FTP from the Cornell University CAC. The multithreaded data transfers from the CAC to McGill are sufficiently fast to maintain 1000–2000 jobs running simultaneously.

When the transfer of an observation is complete, job entries are created in the pipeline's job-tracker database. As compute resources become available, jobs are automatically submitted to the supercomputer's queue.

When jobs terminate, the pipeline checks for results and errors. Failed jobs are automatically re-submitted up to three times to allow for occasional hiccups of the Guillimin task management system, or processing node glitches. If all three processing attempts result in failure, the observation is flagged to be dealt with manually. Observations that are salvageable are re-processed after fixes are applied. The positions of un-salvageable observations are re-inserted into the observing schedule, along with those from observations severely contaminated with RFI. Observations may be un-salvageable if they are aborted scans, contain malformed metadata, or their files have become corrupted. Only ∼0.15% of all observations have data files that cannot be searched, and only ∼4.5% of all observations are flagged to be re-observed due to excessive RFI.

[27] http://arecibo.tc.cornell.edu/PalfaDataPublic
[28] http://www.hpc.mcgill.ca/
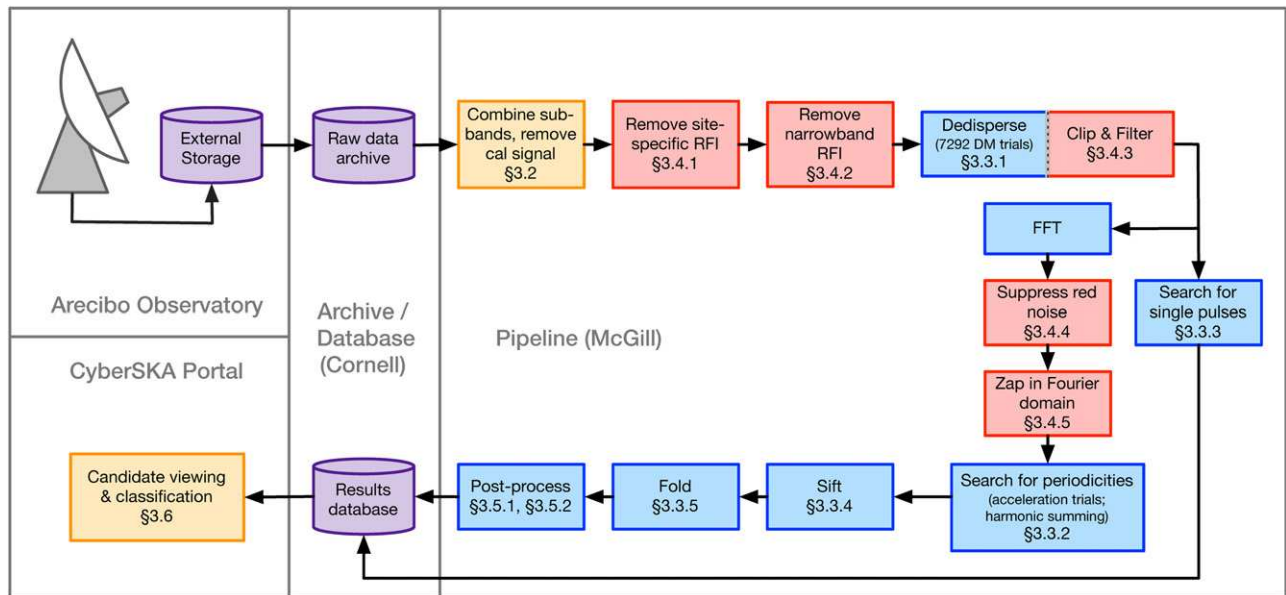[29] https://github.com/plazar/pipeline2.0

Figure 2. Overview of the PALFA survey's `PRESTO`-based pipeline. The color of each element reflects the category of the step: searching is blue; RFI mitigation is red; data storage and databases are purple; miscellaneous processes are yellow. Additional details about each pipeline stage can be found in the sections listed in each box.

The results from successfully processed jobs are parsed and uploaded to a database at the CAC, and the local copies of the data files are removed to free disk space enabling more observations to be requested, downloaded, and analyzed.

The inspection of uploaded results is done with the aid of a web-application (see Section 3.6).

3.2. Pre-processing

Before analyzing the data for astrophysical signals, the two Mock sub-bands must be combined into a single `PSRFITS` file. Each of the two Mock data files have 512 frequency channels, 66 of which are overlapping with the other file. For each sub-integration of the observation, the 478 low-frequency channels from the bottom sub-band and the 480 high-frequency channels from the top sub-band are extracted, concatenated together—along with two extra, empty frequency channels—for each sample, and written into a new full-band data file, consisting of 960 channels. The choice to discard part of both bands was made in order to mitigate the effect of the reduced sensitivity at the extremities of the Mock sub-bands, which causes a slight reduction of sensitivity where they are joined together.

The `PSRFITS` scales and offsets of the Mock sub-bands are adjusted such that the data value levels of top and bottom bands are appropriately weighted with respect to each other.

The combining of the two Mock sub-bands is performed using `combine_mocks` of `psrfits_utils`.[30]

Next, the sub-integrations containing the calibration diode signal are deleted from the observation. The start time and length of the observation are updated accordingly.

At this stage, prior to searching for periodic and impulsive signals, `PRESTO`'s `rfifind` is run on the merged observation to generate an RFI mask. See Section 3.4.2 for details.

3.3. Searching Components

We will now cover the various steps required to search for pulsars and transients.

3.3.1. Dedispersion

Because the DMs of yet-undiscovered pulsars and transients are not known in advance, a wide range of trial DMs must be used to maintain sensitivity to pulsars. For each trial DM value a dedispersed time series is produced by shifting the frequency channels according to the assumed DM value and then summing over frequency. When generating these time series, the motion of the Earth around the Sun is removed so that the arrival times of each sample are referenced to the Solar System barycenter, assuming the coordinates of the beam center.

The PALFA `PRESTO` pipeline searches observations for periodic and impulsive signals up to a DM of $\sim 10,000 \, \mathrm{pc \, cm^{-3}}$. We search to such high DMs despite the maximum DM in our survey region predicted by the `NE2001` model being $\sim 1350 \, \mathrm{pc \, cm^{-3}}$ (Cordes & Lazio 2002) to ensure sensitivity to highly dispersed, potentially extragalactic FRBs (e.g., Thornton et al. 2013; Spitler et al. 2014).

A dedispersion plan is determined by balancing the various contributions to pulse broadening that can be controlled: the duration of each sample (including down-sampling), τ_{samp}; the dispersive smearing within a single channel, τ_{chan}; the dispersive smearing within a single sub-band due to approximating the DM, τ_{sub}; and the dispersive smearing across the entire observing band due to the finite DM step size (i.e., if the DM of the pulsar is half-way between two DM trials), τ_{BW}. Additionally, pulses are broadened by interstellar scattering, τ_{scatt}, which cannot be removed. The amount of scatter-broadening scales with the DM, observing frequency and line of sight. Bhat et al. (2004) empirically determined the

---

Table 3
Dedispersion Plan for Mock Spectrometer Data

DM Range (pc cm^{-3})	DM Step Size (pc cm^{-3})	No. DMs	No. Sub-bands	Sub-band DM Spacing (pc cm^{-3})	Down-sample Factor	Approx. Computing (%)
0–212.8	0.1	2128	96	7.6	1	73.19
212.8–443.2	0.3	768	96	19.2	2	12.20
443.2–534.4	0.3	304	96	22.8	3	8.13
534.4–876.4	0.5	684	96	38.0	5	2.93
876.4–990.4	0.5	228	96	38.0	6	2.44
990.4–1826.4	1.0	836	96	76.0	10	0.73
1826.4–3266.4	2.0	720	96	144.0	15	0.24
3266.4–5546.4	3.0	760	96	228.0	30	0.08
5546.4–9866.4	5.0	864	96	360.0	30	0.05

Note. See also Figure 3 for the pulse broadening as a function of DM due to dispersive smearing and this dedispersion plan.
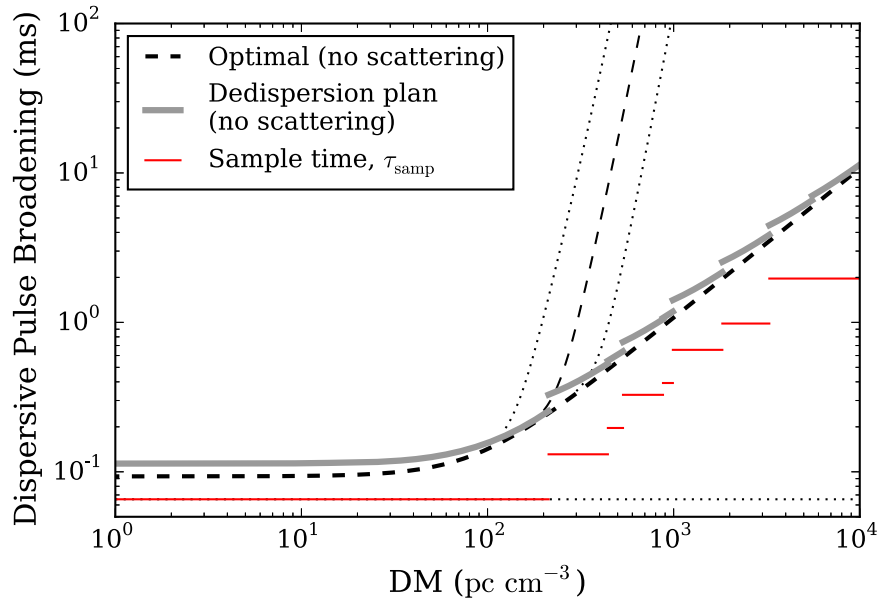

Figure 3. Pulse broadening from down-sampling, and dispersive DM smearing for the dedispersion plan generated by `DDplan.py` shown in Table 3 (gray), as well as the optimal case (dashed black) where neither down-sampling nor smearing from DM errors are included. The optimal case including interstellar scattering is shown (with ± 1 order of magnitude; thin dashed black) assuming the empirical scattering dependence on DM of Bhat et al. (2004). While this dependence is likely reasonable for estimating the scattering of Galactic sources, it is likely to grossly overestimate the scattering of extragalactic sources (e.g., FRBs). In all cases, the middle of the observing band is assumed (∼1375 MHz). Discontinuities are due to down sampling. The horizontal lines (red) show the down sampled time resolution at various DMs.

relationship as

$$\log \tau_{\text{scatt}} = -6.46 + 0.154 \log \text{DM}$$
$$+ 1.07 (\log \text{DM})^2 - 3.86 \log \nu, \quad (1)$$

where τ_{scatt} is given in ms, and ν is the observing frequency in GHz. Even for the same DM, $\log \tau_{\text{scatt}}$ are different for pulsars in different locations with a scatter of up to 2–3 orders of magnitude (Bhat et al. 2004). Because τ_{scatt} cannot (in practice) be corrected, we ignore it when determining our dedispersion plan.

The total correctable pulse broadening, τ_{tot}, is estimated by summing the first four contributions in quadrature,

$$\tau_{\text{tot}} = \sqrt{\tau_{\text{samp}}^2 + \tau_{\text{chan}}^2 + \tau_{\text{sub}}^2 + \tau_{\text{BW}}^2}. \quad (2)$$

All of these broadening terms vary with DM. The dedispersion plan is chosen to equate these four broadening effects roughly by adjusting the DM step-size and down-sampling factor as a function of DM. To reduce the number of DM trials, the minimum step-size is determined by $\tau_{\text{BW}} > 0.1$ ms.

The PALFA survey dedispersion plan for Mock spectrometer data was determined with a version of PRESTO's `DDplan.py` modified to allow for non-power-of-two downsampling factors, and is shown in Table 3. The down-sampling factors are selected to be divisors of the number of spectra per sub-integration, 15,270. The amount of dispersive smearing incurred at the middle of the observing band, ∼1375 MHz, when using the dedispersion plan in Table 3, ranges from ∼0.1 ms for the lowest DMs, to ∼1 ms for DMs of a few 100 pc cm^{-3}, increasing to ∼10 ms for a DM of ∼10,000 pc cm^{-3}. Above a DM of ∼500 pc cm^{-3} scattering begins to dominate (see Figure 3).

The more aggressive down-sampling at higher DMs has the advantage of reducing the data size, making the analysis more efficient. Also, at higher DMs the step-size between successive DM trials is increased, further reducing the amount of processing. Therefore, the extra computing required to go to

high DMs is relatively small compared to what is required to search for pulsars and transients at low DMs. Searching DMs between 1000 and 10,000 pc cm^{-3} adds only ~5% the total data analysis time.

Dedispersion is done with `PRESTO`'s `prepsubband`, passing through the raw data 99 times, and resulting in 7292 dedispersed time series. In all cases `prepsubband` internally uses 96 sub-bands, each of 10 MHz, for its two-stage sub-band dedispersion process. Time intervals containing strong impulsive RFI are removed by `prepsubband`, as prescribed by a RFI mask (see Section 3.4.2).

A second set of dedispersed time series are created as before, but also applying a version of the zero-DM filtering technique described by Eatough et al. (2009) that has been augmented to use the bandpass shape when removing the zero-DM signal from each channel. These zero-DM filtered time series are especially useful for single-pulse searching, which is described in Section 3.3.3. See Section 3.4.3 for details on time-domain RFI mitigation strategies used.

Dedispersion makes up roughly 15%–20% of the processing time.

3.3.2. Periodicity Searching

For every dedispersed time series, the discrete Fourier transform (DFT) is computed using `PRESTO`'s `realfft`. Prior to searching the DFT for peaks, it is normalized to have unit mean and variance. The normalization algorithm is designed mainly to suppress red noise (i.e., low-frequency trends in the time series; for more details see Section 3.4.4). Also, Fourier bins likely to contain interference are replaced with the median-value of nearby bins. Details of the algorithm used to determine RFI-prone frequencies are described in Section 3.4.5.

Two separate searches of the DFT are conducted using `PRESTO`'s `accelsearch`. Both searches identify peaks in the DFT down to a frequency of 0.125 Hz.

The first, *zero-acceleration*, search is tuned to identify isolated pulsars. The power spectrum of the signal from an isolated pulsar will consist of narrow peaks at the rotational frequency of the pulsar and at harmonically related frequencies. The number of significant harmonics depends on the width of the pulse profile, W, and the spin period, P, as $N_{\mathrm{harm}} \sim P/W$. To improve the significance of narrow signals, power from harmonics is summed with that of the fundamental frequency. The zero-acceleration search sums up to 16 harmonics, including the odd harmonics, in powers of 2 (i.e., 1, 2, 4, 8, 16 harmonics). For signals with significant higher harmonics, this harmonic summing procedure also improves the precision of the detected frequency.

The second, *high-acceleration*, search is optimized to find pulsars in binary systems. The time-varying line of sight velocity of such pulsars gives rise to a Doppler shift that varies over the course of an observation. This smears the signal over multiple bins in the Fourier domain. To recover sensitivity to binary pulsars we use the Fourier-domain acceleration search technique described in Ransom et al. (2002). In short, the high-acceleration search performs matched-filtering on the DFT using a series of templates each corresponding to a different constant acceleration. We search using templates up to 50 Fourier bins wide, which corresponds to a maximum acceleration of ~ 1650 m s^{-2} for a 5-minute observation of a 10-ms pulsar. Only up to 8 harmonics are summed in the high-

acceleration case because of its larger computational requirements.

For each of the periodic signal candidates identified in both the zero- and high-acceleration searches we interpolate the frequency and frequency derivative (i.e., acceleration) to optimize the harmonics. We then normalize the harmonics, and compute the equivalent Gaussian significance of the candidate, σ_F, based on the probability of seeing a noise value with the same amount of incoherently summed power (see Ransom et al. 2002, for details). The zero- and high-acceleration candidate information is saved to separate lists for later post-processing. We record information candidates with $\sigma_F > 2$ for the zero-acceleration search. For the high-acceleration search we use a slightly larger threshold of $\sigma_F > 3$ to partially compensate for the increased number of trials. However, due to the large number of candidates resulting from searching all DM trials, we only consider those with $\sigma_F > 6$ for folding (see Section 3.3.4 for details).

Typically, the zero-acceleration and high-acceleration searches make up between 2–5% and ~30% of the overall computation time, respectively.

3.3.3. Single Pulse Searching

Each dedispersed time series is also searched with `PRE-STO`'s `single_pulse_search.py` for impulsive signals with a matched-filtering technique (e.g., Cordes & McLaughlin 2003). Prior to searching, the time series is detrended by subtracting the linear slope from each 1000-sample block. The standard deviation of each block, σ_{block} is estimated.[31] To identify single pulse candidates, multiple box-car templates corresponding to a range of durations up to 0.1 s are used.[32] Candidate single-pulse events at brighter than $5\,\sigma_{\mathrm{block}}$ are recorded. Diagnostic plots featuring only $>6\,\sigma_{\mathrm{block}}$ candidate events are generated and archived for later viewing. In addition to the basic diagnostic plots, all of the $>5\,\sigma_{\mathrm{block}}$ events are used in post-processing algorithms designed to distinguish astrophysical signals (e.g., from pulsars/RRATs and extragalactic FRBs) from RFI and noise. The algorithms employed by PALFA are described elsewhere (Spitler 2013; Karako-Argaman et al. 2015).

The same searching and post-processing procedure is also applied to zero-DM filtered time series. To filter the data, we employ an enhanced version of what was originally described in Eatough et al. (2009). See Section 3.4.3 for more details about the time-domain RFI-mitigation techniques used.

The single-pulse searching makes up approximately 20% of the computing time.

3.3.4. Sifting

As described above, the output of periodicity searching is a set of files, the zero- and high-acceleration candidate lists for each DM trial, containing the frequency of significant peaks found in the Fourier transformed time series, along with other information about the candidate. In total, for all DMs, there are typically $\sim 10^4$ period-DM pairs per beam. These signal

---

[31] In `single_pulse_search.py`, the standard deviation calculation excludes the 2.5% largest values and the 2.5% smallest values in the block. The standard deviation is corrected for the discarded data assuming the remaining values are Gaussian distributed.

[32] The possible widths of the templates are 1, 2, 3, 4, 6, 9, 14, 20, 30, 45, 70, 100, 150, 220, 300 bins. The largest template used depends on the resolution of the time series and the <0.1 s restriction.

candidates are *sifted* to identify the most promising pulsar candidates, match harmonically related signals, and reject RFI-like signals.

The first stage of the sifting process is to remove short-period candidate signals ($P < 0.5$ ms), which contribute a large number of false-positives, as well as to ensure no candidate signals with periods longer than the limit of our search ($P > 15$ s) are present. Weak candidates with Fourier-domain significances $\sigma_F < 6$ are also removed. Furthermore, candidates with weak or strange harmonic powers are rejected if they match one of the following cases: (1) the candidate has no harmonics whose power is at least 8 times larger than the local power spectrum level; (2) the candidate has $\gtrsim 8$ harmonics and is dominated by a high harmonic (fourth[33] or higher), having at least twice as much power as the next-strongest harmonic; (3) the candidate has 4 harmonics and is dominated by a high harmonic (third or higher), having at least three times as much power as the next-strongest harmonic.

The next stage of sifting is to group together candidates with similar periods (at most 1.1 Fourier bins apart) found in different DM trials. When a duplicate period is found, the less significant candidate is removed from the main list, and its DM is appended to a list of DMs where the stronger candidate was detected.

At this stage, for each periodic signal, there is a list of DMs at which it was detected. The next step is to purge candidates with suspect DM detections. Specifically, candidates not detected at multiple DMs, candidates that were most strongly detected at DM $\leqslant 2$ pc cm^{-3}, and candidates that were not detected in consecutive DM trials are all removed from subsequent consideration.

The steps described above are applied separately to candidates found in the zero- and high-acceleration searches. At this point, the two candidate lists are merged, and signals harmonically related to a stronger candidate are removed from the list. This process checks for a conservative set of integer harmonics, and small integer ratios between the signal frequencies. As a result, some harmonically related signals are occasionally retained in the final candidate list.

The sifting process typically results in ~ 200 good candidates per beam, of which ~ 100 are above the significance threshold for folding. The fraction of time spent on candidate sifting is negligible ($<0.1\%$) compared to the rest of the pipeline.

3.3.5. Folding

The raw data are folded for each periodicity candidate with $\sigma_F \geqslant 6$ remaining after the sifting procedure using PRESTO's `prepfold`. At most 200 candidates are folded for each beam. In more than 99% of cases this limit is sufficient to fold all $\sigma_F \geqslant 6$ candidates. If too many candidates have $\sigma_F \geqslant 6$, the candidates with largest σ_F are folded.

After folding, `prepfold` performs a limited search over period, period-derivative, and DM to maximize the significance of the candidate. However, for candidates with $P > 50$ ms the search over DM is excluded because it is prone to selecting a strong RFI signal at low DM even if there is a pulsar signal present. Furthermore, the optimization of the period-derivative is also excluded for $P > 500$ ms candidates.

For each folded candidate a diagnostic plot is generated (see Ransom 2001, for examples). These plots, along with basic information about the candidate (optimized parameters, significance, etc.) are placed in the PALFA processing results database, hosted at the Cornell CAC. The `prepfold` binary output files generated for each fold are also archived at Cornell.

The binary output files created by `prepfold` are used by a candidate-ranking artificial intelligence (AI) system, as well as to calculate heuristics for candidate sorting algorithms. Details can be found in Section 3.5.

Folding the raw data for up to 200 candidates per beam is a considerable fraction ($\sim 25\%$) of the overall computing time.

3.4. RFI-mitigation Components

The sensitivity of Arecibo and PALFA can only be fully realized if interference signals in the data are identified and removed. To work toward this goal, the PALFA pipeline includes multiple levels of RFI excision. Each algorithm is designed to detect and mitigate a different type of terrestrial signal. Because these interference signals are terrestrial they are not expected to show the $1/f^2$ frequency sweep characteristic of interstellar signals. Unfortunately, some terrestrial signals show broadband frequency sweeps that cannot be distinguished from astronomical signals by data analysis pipelines (e.g., "perytons" Burke-Spolaor et al. 2011; Petroff et al. 2015). Despite some non-astronomical signals remaining in the data, the suite of RFI-mitigation techniques described here are an essential part of the pipeline.

All of the algorithms described here are applied to non-dedispersed, topocentric data.

3.4.1. Removal of Site-specific RFI

Unfortunately, some of the electronics hardware at the Arecibo Observatory, specifically the ALFA bias monitoring system,[34] introduced strong periodic interference into our data. By the time the source of the interference was determined several months of observations had been affected. Fortunately, we were able to develop a finely tuned algorithm to excise the signal using our knowledge of the sub-pulse structure to identify and remove these intense bursts of interference. The removed sections of data are replaced with a running median, which is computed separately for each ~ 1 s block of data. Finely tuned algorithms such as this one have the advantage of more easily identifying specific RFI signals and only extracting the affected data. In this particular case, each 1 s burst of RFI is made up of a comb of ~ 10 ms-long sub-pulses repeated every ~ 50 ms. By removing these bursts, our algorithm largely eliminates the broad peaks in the Fourier domain that are introduced by the pernicious electronics, typically between 1 and 1000 Hz (i.e., exactly where we expect pulsars to be found). See Figure 4 for an example. Furthermore, by removing the interference pulses in the time domain, the power spectrum is cleaned without sacrificing any intervals of the Fourier domain, as would be the case with the zapping algorithm described in Section 3.4.5.

Because the equipment causing the bursts of interference in our observations is not essential to data taking we have been able to shut it off during PALFA sessions.

---

[33] We number harmonics such that the frequency of the Nth harmonic is N times larger than the fundamental frequency.

[34] The ALFA bias monitoring system measures the amplifier bias voltages, as well as other systems in the dewars, including temperatures, currents, and voltages.
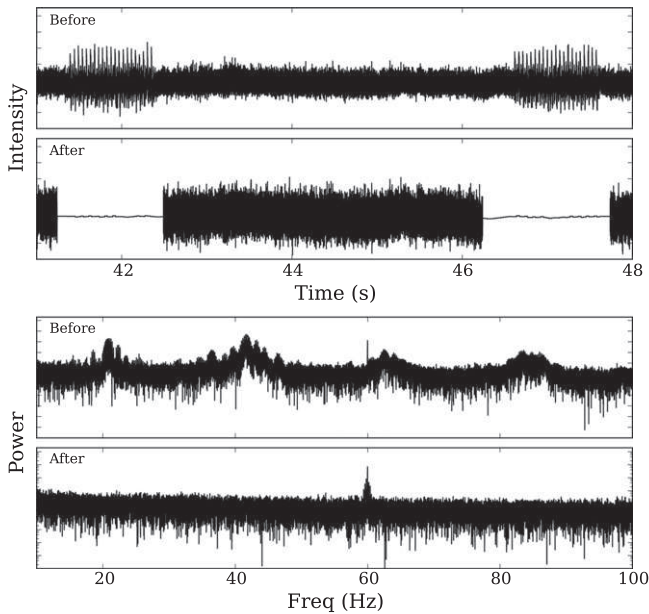
Figure 4. Example of the effect of the bursts of interference caused by some of the electronics equipment at the Arecibo Observatory on PALFA survey data in time and frequency domain (labeled "Before") and the same interval of time series and power spectrum after our finely tuned removal algorithm, described in Section 3.4.1, is applied (labeled "After"). Part of the time series is sacrificed, but the broad features in the frequency domain are completely removed. The RFI peak at 60 Hz that remains in the bottom panel is caused by the electrical mains and is later removed by zapping intervals of the power spectrum (described in Section 3.4.5). The source of this interference signal has been identified and can be dealt with by shutting it off during PALFA observations. The linear slope in the power spectrum is due to red noise in the PALFA data. The effect of red noise is discussed in Sections 6 and 7.

3.4.2. Narrow-band Masking

Every observation is examined for narrow-band RFI signals using PRESTO's rfifind, which considers 2 s long blocks of data in each frequency channel separately. For each block of data two time-domain statistics are computed: the mean of the block data value, and the standard deviation of the block data values. Also, one Fourier-domain statistic is computed for each block: the maximum value in the power spectrum. Blocks where the value of one or more of these three statistics is sufficiently far from the mean of its respective distribution are flagged as containing RFI. For the two time-domain metrics, in the PALFA survey the threshold for flagging a block is 10 standard deviations from the mean of the distribution, and for the Fourier-domain metric, the threshold is 4 standard deviations from the mean. The resulting list of flagged blocks is used to mask out RFI. Masked blocks are filled with constant data values chosen to match the median bandpass of that time interval. Sub-integrations that are at least 70% masked are completely replaced. Similarly, channels that are more than 30% masked are completely replaced with zeros.

On average, only ~5.75% of time-frequency space is masked by this algorithm, and ~93% of observations have mask-fractions less than 10%. Having a mask-fraction larger than 15% is one of the conditions used to identify observations that will be re-inserted into the list of sky positions to observe. Only ~1.1% of observations fall into this category.

The fraction of data masked for each beam, and a graphical representation of the mask are stored in the results database as diagnostics of the observation quality.
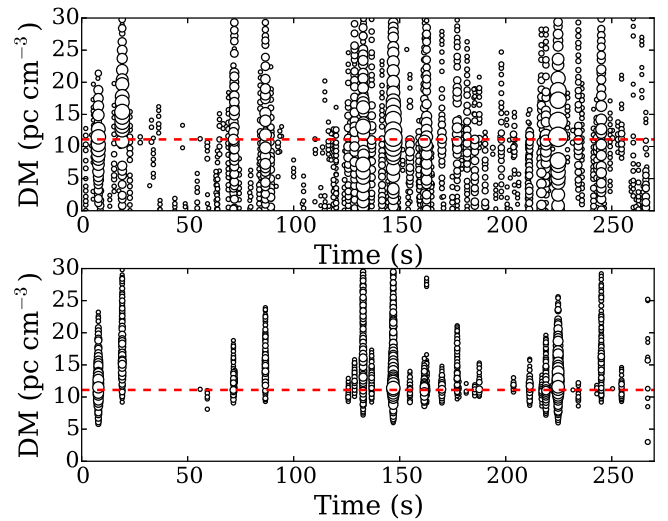

Figure 5. Comparison of single-pulse events detected in a PALFA observation of PSR J1908+0734 in a search of the un-filtered time series (top) and the zero-DM filtered time series (bottom). Each circle represents the time and DM of an impulsive signal found by PRESTO's single_pulse_search.py. The size of the circle is proportional to the significance of the signal (up to a maximum radius). Most of the RFI is filtered out of the observation by the zero-DM algorithm while leaving the pulsar pulses, albeit with some loss of significance at the lower DMs (see Eatough et al. 2009, for a discussion). Thus, the zero-DM filtering technique makes it far easier to disentangle astrophysical signal at non-zero DMs from RFI at DM = 0 pc cm^{-3} both by eye and algorithmically. The pulsar's DM = 11 pc cm^{-3} is indicated with the dashed red line.

Generating the rfifind mask makes up only ~1% of the total pipeline running time.

3.4.3. Time-domain Clipping and Filtering

It is possible for broad-band impulsive interference signals to be missed by the masking procedure described above if the signals are not sufficiently strong to be detected in individual channels. Fortunately, the PALFA pipeline makes use of a complementary algorithm designed to remove such signals from the data: a list of bad time intervals is determined by identifying samples in the DM = 0 pc cm^{-3} time series that are significantly larger ($>6\,\sigma_{\rm loc}$) than the surrounding data samples. The spectra corresponding to the bad time intervals are replaced by the local median bandpass.

As previously mentioned, for single-pulse searching, the PALFA pipeline also applies the PRESTO-implementation of the zero-DM filtering technique described in Eatough et al. (2009). This implementation enhances the original prescription by using the bandpass shape as weights when removing the DM = 0 pc cm^{-3} signal. The zero-DM filter greatly reduces the impact of RFI on single-pulse searching, facilitating low-DM RRATs being distinguished from RFI. To illustrate the benefits of zero-DM filtering, Figure 5 shows a comparison of the single-pulse events identified by single_pulse_search.py in an observation of PSR J1908+0734 with and without filtering.

3.4.4. Red-noise Suppression

In order to properly normalize the power spectrum and compute more correct false-alarm probabilities (see Ransom et al. 2002), we use a power spectrum whitening technique to suppress frequency-dependent, and in particular "red" noise.
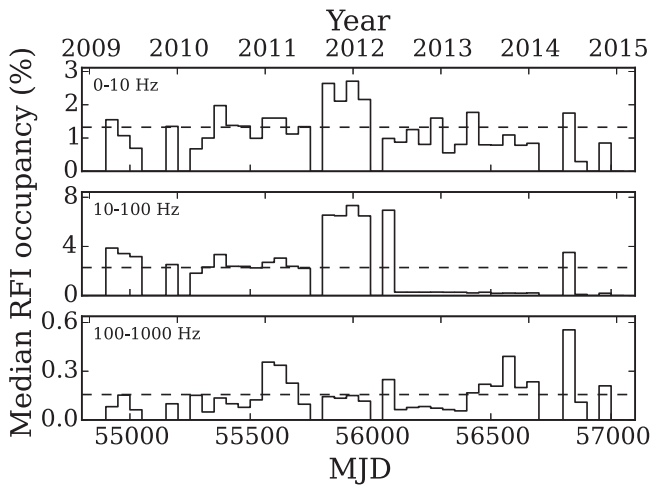
Figure 6. Median percentage of the Fourier domain occupied by RFI in three frequency ranges for 50-day intervals (solid lines) compared against the median percentage for all observations (dashed lines). Many periodic sources of RFI are found to vary on daily timescales. Thus, lists of RFI-contaminated Fourier frequencies to be removed from the power spectrum prior to searching are tailored to the RFI of each MJD. The increase in RFI in the middle panel between MJD 55750 and 56100 was due to on-site electronics at the telescope, which since being identified in 2012 June (MJD $\simeq$ 56100) have nearly always been turned off during PALFA observations, significantly reducing the RFI in the 10–100 Hz interval.

The median power level is measured in blocks of Fourier frequency bins and then divided by log 2 to convert the median level to an equivalent mean level assuming that the powers are distributed exponentially (i.e., χ^2 with 2 degrees-of-freedom).

The number of Fourier frequency bins per block is determined by the log of the starting Fourier frequency bin, beginning with 6 bins and increasing to approximately 40 bins by a frequency of 6 Hz. Above that frequency, where there is little to no "colored" noise, block sizes of 100 bins are used. The resulting filtered power spectrum has unit mean and variance. This process is accomplished with PRESTO's `rednoise` program.

3.4.5. Fourier-domain Zapping

Sufficiently bright periodic sources of RFI can be mistakenly identified as pulsar candidates by our FFT search. To excise, or *zap*, these signals from our data we tabulate frequency ranges often contaminated by RFI. The Fourier bins contained in this *zap list* are replaced by the average of nearby bins prior to searching.

The RFI environment at Arecibo is variable. The number, location, and width of interference peaks in the Fourier transform of DM $= 0$ pc cm^{-3} time series vary on a timescale of months to years. To demonstrate this, the fraction of Fourier bins occupied by RFI as a function of epoch is illustrated in Figure 6. The median fraction of the Fourier spectrum occupied by RFI for all Mock spectrometer data for various intervals is: 2.9% (0–10 Hz), 5.1% (10–100 Hz), and 0.5% (100–1000 Hz). To account for this dynamic nature of the RFI, we compute zap lists for each MJD.

To compute zap lists we exploit the fact that RFI signals are typically detected by multiple feeds in a single 5 minute pointing, or persist for most of an observing session (typically 1–3 hr). The strategy we employ here is similar to what was used in the Parkes Multibeam Pulsar Survey (Manchester

et al. 2001). Fourier bins contaminated by RFI are determined by finding peaks in a *median power spectrum*, which is comprised of the bin-wise median of multiple DM $= 0$ pc cm^{-3} power spectra. This is done twice, using two different subsets of data: (a) all observations made with a given ALFA feed on a given day (to identify RFI signals that persist for multiple hours, or issues specific to the ALFA receiver), and (b) all seven observations from a given pointing (to identify shorter-duration periodic RFI signals that enter multiple feeds). The zap list for any given observation is the union of the lists for its pointing and its feed.

Observations whose power spectra are more than 8% occupied by RFI are flagged for re-observation. Roughly 3% of observations meet this criterion.

With the advent of sophisticated candidate ranking and candidate classifying machine-learning algorithms (see Section 3.5), it is better to leave some RFI in the data than to remove large swaths of the Fourier domain. To avoid excessive zapping we remove at most 3% from each frequency decade, up to a maximum of 1% globally, preferentially zapping bins containing the brightest RFI.

In addition to being an essential part of the PALFA RFI-mitigation strategy, zap lists have also proven to be a useful diagnostic for monitoring the RFI environment at Arecibo.

3.5. Post-processing Components

3.5.1. Ratings

A series of 19 heuristic ratings are computed for each folded periodicity candidate produced by the data analysis pipeline. These ratings encapsulate information about the shape of the profile, the persistence and broadbandedness of the signal, whether the frequency of the signal is particularly RFI-prone, and whether the signal is stronger at DM $= 0$ pc cm^{-3}. Each of the ratings is uploaded to the results database, and is available for querying and sorting candidates (see Section 3.6). The ratings and brief descriptions are presented in Table 4.

The ratings are incorporated into candidate-selection queries along with standard parameters such as period, DM, and various measures of time-domain and frequency-domain significance. Using ratings in this way allows users to constrain the candidates they view to have certain features they would require when selecting promising candidates by eye. Alternatively, the ratings have been used in a decision-tree-based AI algorithm, but this has since been supplanted by the more sophisticated "Pulsar Image-based Classification System (PICS)" algorithm described in Section 3.5.2 (Zhu et al. 2014).

The code to compute the ratings[35] is compatible with the binary files produced by PRESTO's `prepfold` for each periodicity candidate. For each candidate a text file is written containing the name, version, description, and value for all ratings being computed. This task is performed as part of the data analysis pipeline. The rating information is later uploaded to the results database. In cases where a new rating is devised, or an existing rating is modified, the `prepfold` binary files are fetched from the results archive, ratings are computed in a stand-alone process (i.e., independent of the pipeline), and the values are inserted into the database. The values of improved ratings are inserted alongside values from old versions to permit detailed comparisons.

---

[35] Available at https://github.com/plazar/ratings2.0.

Table 4
Heuristic Candidate Ratings

Rating	Description
Profile Ratings[a]	
Duty Cycle	Fraction of profile bins larger than half the maximum value of the profile
Peak Over rms	Maximum value of the profile divided by the RMS
Profile Ratings (Gaussian Fitting)[a]	
Amplitude	Amplitude of a single Gaussian component fit to the profile
Single Component GoF	Goodness of Fit of a single Gaussian component fit to the profile
FWHM	Full-width at half-maximum of a single Gaussian component fit to the profile
No. Components	Number of Gaussian components required to acceptably fit the profile (up to 5 components)
Multi-component GoF	Goodness of fit of the multiple Gaussian component fit (up to 5 components)
Pulse Width	Ratio of narrowest component of the multiple Gaussian fit compared to the pulse broadening (excluding scattering)
Time versus Phase Ratings	
Period Stability	Fraction of good time intervals that deviate in phase by $\leqslant 0.02$
Frac. of Good Sub-ints	Fraction of time intervals that contain the pulsar signal
Sub-int. SNR Variability	The standard deviation of sub-integration S/Ns
Frequency versus Phase Ratings	
Frac. of Good Sub-bands	Fraction of sub-bands that contain the pulsar signal
Sub-band SNR Variability	The standard deviation of sub-band S/Ns
DM Ratings	
DM Comparison (standard deviation)	Ratio of the standard deviation of the profile at $DM = 0$ pc cm^{-3} and at the optimal DM
DM Comparison (χ^2)	Ratio of the χ^2 of the profile at $DM = 0$ pc cm^{-3} and at the optimal DM
DM Comparison (peak)	Ratio of the peak value of the profile at $DM = 0$ pc cm^{-3} and at the optimal DM
Miscellaneous Ratings	
Known Pulsar	A measure of how similar the candidate period and DM are to a nearby pulsar (also checks harmonic relationships)
Mains RFI	A measure of how close the topocentric frequency is to 60 Hz, or a harmonic
Beam Count	The number of beams from the same pointing containing another candidate with the same period

Notes. See Section 3.5.1 for more details on how ratings are used to select candidates.
[a] Prior to computing ratings, the profile is normalized such that the median level is 0 and the standard deviation is 1.

3.5.2. Machine Learning Candidate Selection

All periodicity candidates are also assessed by the PICS (Zhu et al. 2014), an image-pattern-recognition-based machine-learning system for selecting pulsar-like candidates. The PICS deep neural network enables it to recognize and learn patterns directly from 2D diagnostic images produced for every periodicity pulsar candidate. The large variety of pulsar candidates used to train PICS has developed its ability to recognize both pulsars and their harmonics.

PICS can reduce the number of candidates to be inspected by human experts by a factor of ∼100 while still identifying 100% of pulsars and 94% of harmonics to the top 1% of all candidates (Zhu et al. 2014).

Since late 2013, PICS has been integrated directly into the PALFA processing pipeline. It produces a single rating for each candidate, which is uploaded into the results database as a rating (see Section 3.5.1). So far, this has aided in the discovery of 8 pulsars (see Section 4).

3.5.3. Coincidence Matching

While PALFA has been successful at finding moderately bright MSPs, the vast quantity of periodicity candidates close to the detection threshold at very short periods ($\lesssim 2$ ms) have made it more challenging to identify the *faint* MSPs in the PALFA results database. To facilitate the process, a search for signals with compatible periods, DMs, and sky positions has been performed on the periodicity candidates in the database. By applying our coincidence matching algorithm to the complete list of folded candidates we are able to reliably probe lower S/Ns than would be reasonable to do thoroughly by manual viewing. This algorithm is complementary to our machine learning technique that operates on each candidate individually. The software developed to find matching candidates is available on the web for general use.[36]

Large parts of the survey region have either been observed more than once or have been densely sampled (see Figure 1),

---

[36] https://github.com/smearedink/PALFA-coincidences

making it possible to match the detection of a pulsar from multiple observations confidently. For each observation, a list of beams from other pointings that fall within 5′ is generated. Candidates from the different beams are matched by their DMs and barycentric periods. Allowances are made for slightly different DMs and periods, as well as for harmonically related periods. Multiple matches that include the same candidate are consolidated to form groups of more than two candidates.

The results of this matching algorithm are examined with a dedicated, web-based interface. Many known pulsars, especially high harmonics of very bright slow pulsars, have already been identified.

As of 2015 January, our coincidence matching search has not yet resulted in the discovery of new pulsars, but it continues to be applied to the results database. This algorithm will be increasingly useful as more of the PALFA survey region becomes densely sampled, and as more Mock spectrometer observations cover positions previously observed with the WAPP spectrometers.

3.6. Collaborative Tools

The PALFA Consortium has created and made use of several online collaborative tools on the CyberSKA portal[37] (Kiddle et al. 2011), a website developed to help astronomers build tools and strategies for large-scale projects in the lead-up to the Square Kilometre Array (SKA).

The CyberSKA portal allows for third-party applications to be accessed directly without a need for separate user authentication. Within this framework several PALFA-specific applications were developed:

Candidate Viewer—The primary method for viewing and classifying PALFA candidates is by using the CyberSKA *Candidate Viewer* application. It allows users to access the Cornell-hosted results database using form-based, free-text, and saved queries. Queries include basic observation and candidate information (e.g., sky position, period, DM, significance), as well as ratings (Section 3.5.1), and the PICS classifications (Section 3.5.2). Users are presented with a series of `prepfold` diagnostic plots in sequence, one for each candidate matching the query. By inspecting the plots, as well as other relevant information provided, such as a histogram showing the number of occurrences of signals in the relevant frequency range as well as a summary plot showing all the beam's periodic signal candidates in a period-DM plot, the user can quickly classify candidates. Classifications are saved to the database and can be easily retrieved.

Top Candidates—Especially promising candidates found with the Candidate Viewer can be added to the *Top Candidates* application, which is designed to store the most likely pulsar candidates. The application also allows collaboration members to view and vote on which candidates should be subject to confirmation observations, as well as help organize and track these observations and their outcomes.

Survey Diagnostics—Optimizing the use of telescope time and computing resources is extremely important for large-scale pulsar surveys such as PALFA. The *Survey Diagnostics* application automatically compiles a set of information and a set of plots from various sources to help the project run smoothly. This includes the status of data acquisition and

---

[37] http://www.cyberska.org

reduction, the severity of the RFI environment, and the quality of the data.

4. RESULTS

The PALFA Survey has discovered 144 pulsars, including 19 MSPs and 11 RRATs, and one FRB, as of 2015 March. The `PRESTO`-based pipeline described in Section 3 has discovered 40 pulsars from their periodic emission, 5 RRATs from their impulsive emission, and re-detected another 60 pulsars that were previously discovered with other PALFA data analysis pipelines. The other pulsars found in the PALFA survey were discovered with the different data analysis pipelines, such as the E@H and Quicklook pipelines (Allen et al. 2013; Stovall 2013) which use complementary RFI-excision and search algorithms, with dedicated transient searches, or in earlier observations with the WAPP spectrometers using an earlier version of the pipeline described here. Not all sky positions observed with the WAPP spectrometers have been covered with the Mock spectrometers yet.

We report details for 40 of the periodicity-discovered pulsars found in Mock spectrometer data with the pipeline described above. All but one of these discoveries are in the inner Galaxy region. These pulsars were discovered by analyzing 85,333 beams, covering a total of 134 sq. deg., which consists of 80 sq. deg. in the inner Galaxy region, and 54 sq. deg. in the outer Galaxy region (see Table 2). Basic parameters of the discoveries are in Table 5, and pulse profiles from the discovery observations are shown in Figure 7.

Eight of the 40 pulsars reported here are MSPs, including the most distant MSP (based on its DM) discovered to date, PSR J1850+0242. The distance estimated from the DM of PSR J1850+0242, assuming the NE2001 model (Cordes & Lazio 2002), is 10.4 kpc, a testament to the ability of the PALFA survey to find highly dispersed, short period pulsars. PSR J1850+0242, along with three of the other MSPs discoveries reported here are described in detail in Scholz et al. (2015). Three more of the MSPs reported here will be included in K. Stovall et al. (2015, in preparation).

Nine of the 40 pulsars reported here are in binary systems, including seven of the MSPs, and two slower pulsars, PSRs J1932+17 ($P \simeq 42$ ms) and J1933+1726 ($P \simeq 22$ ms), which have small spin-down rates, indicating they were spun-up by the accretion of mass and transfer of angular momentum, the so-called "recycling" process (Alpar et al. 1982). The timing analyses of PSRs J1932+17 and PSR J1933+1726 will be provided by E. Madsen et al. (2015, in preparation) and K. Stovall et al. (2015, in preparation), respectively.

Timing solutions for six of the slow pulsars presented in this work, including the young PSR J1925+1721, will be published in a forthcoming paper along with the timing of other PALFA-discovered pulsars (A. G. Lyne et al. 2015, in preparation).

In addition to the 40 pulsars detailed here that were discovered in periodicity searches, the `PRESTO`-based pipeline has found 5 RRATs. The beams containing these RRATs were identified using a post-processing algorithm originally developed for pulsar surveys at 350 MHz with the Green Bank Telescope (see Karako-Argaman et al. 2015, for details). Discovery parameters and detailed follow-up observations for these RRATs will be described elsewhere.

Table 5
Pulsars Discovered in Mock Spectrometer Data with the PRESTO Pipeline

Name	Disc. Period (ms)	Disc. DM (pc cm^{-3})	Disc. Significance (σ_F)	Flux Density[a] (mJy)
J0557+1550[b]	2.55	102.7	8.34	0.050(6)[c]
J1850+0242[b]	4.48	540.5	13.08	0.33
J1851+0232	344.02	605.4	10.82	0.09
J1853+03	585.53	290.2	14.28	...[d]
J1854+00[e]	767.33	532.9	10.44	...[d]
J1858+02	197.65	492.1	14.91	...[d]
J1901+0235[e]	885.24	403.0	26.7	...[d]
J1901+0300[b]	7.79	253.7	11.8	0.113(4)[c]
J1901+0459	877.06	1103.6	10.93	0.10
J1902+02[e]	415.32	281.2	7.58	...[d]
J1903+0415[e]	1151.39	473.5	12.48	...[d]
J1904+0451[b]	6.09	183.1	8.78	0.117(9)[c]
J1906+0055	2.79	126.9	16.47	0.12
J1906+0725	1536.51	480.4	7.13	0.05
J1907+0256	618.77	250.4	12.07	0.19
J1907+05	168.68	456.7	10.0	...[d]
J1909+1148	448.95	201.9	15.93	0.06
J1910+1027	531.47	705.7	9.29	0.06
J1911+09	273.71	334.7	7.13	...[d]
J1911+10	190.89	446.2	7.48	...[d]
J1913+0617	5.03	155.8	9.81	...[d]
J1913+1103	923.91	628.9	9.86	0.09
J1914+0659	18.51	224.7	12.66	0.33
J1915+1144	173.65	338.3	23.59	0.08
J1915+1149	100.04	702.1	7.58	...[d]
J1918+1310	856.74	247.4	6.56	...[d]
J1921+16	936.43	204.7	8.13	...[d]
J1924+1628[e]	375.09	542.9	21.12	0.09
J1924+17	758.43	527.4	10.66	...[d]
J1925+1721	75.66	223.7	16.06	0.09
J1926+1613[e]	308.30	32.9	14.9	...[d]
J1930+14[e]	425.71	209.2	12.15	0.04
J1931+1440	1779.23	239.3	23.63	0.12
J1932+17[e]	41.82	53.2	12.89	...[d]
J1933+1726	21.51	156.6	7.28	0.04
J1934+19	230.99	97.6	18.67	0.10
J1936+20	1390.88	205.1	6.6	...[d]
J1938+2012[e]	2.63	237.1	8.55	0.02
J1940+2246	258.89	218.1	14.47	0.09
J1957+2516	3.96	44.0	6.61	0.04

Notes.
[a] Phase-averaged flux density. Determined using the radiometer equation (see Section 4.1) unless otherwise noted.
[b] Pulsar was previously published by Scholz et al. (2015).
[c] Flux calibrated using noise diode. Value from Scholz et al. (2015).
[d] Refined position not available. Flux density could not be estimated.
[e] Pulsar was first identified using the PICS machine learning candidate selection system described in Section 3.5.2.

4.1. Estimating Flux Densities of New Discoveries

The flux densities of the new discoveries were estimated using the radiometer equation (Dewey et al. 1985),

$$S_{est} = \frac{(S/N)_T \left(T_{sys} + T_{sky}\right)}{G\left(\theta, ZA\right)\sqrt{n_p t_{obs}\Delta f}} \sqrt{\frac{W}{P - W}}, \qquad (3)$$

where relevant parameters are the pulse profile width, W, the telescope gain, $G(\theta, ZA)$, the number of polarization channels summed, n_p, the observation length, t_{obs}, the observing bandwidth, Δf, the period of the pulsar, P, the system and

sky temperatures, T_{sys} and T_{sky}, respectively. The time-domain S/N, $(S/N)_T$, was measured from folded profiles using the area under the pulse and the off-pulse RMS.

In some cases, predominantly for long-period pulsars, the baseline of the pulse profile exhibited broad features, likely due to red noise. (See some examples in Figure 7.) To more robustly estimate flux densities, we fit Gaussian components to the pulse profile, including the broad off-pulse features. The integrated pulsar signal was determined from the on-pulse components, and the noise level of the profile was determined from the standard deviation of the residuals after subtracting all fitted components from the profile.
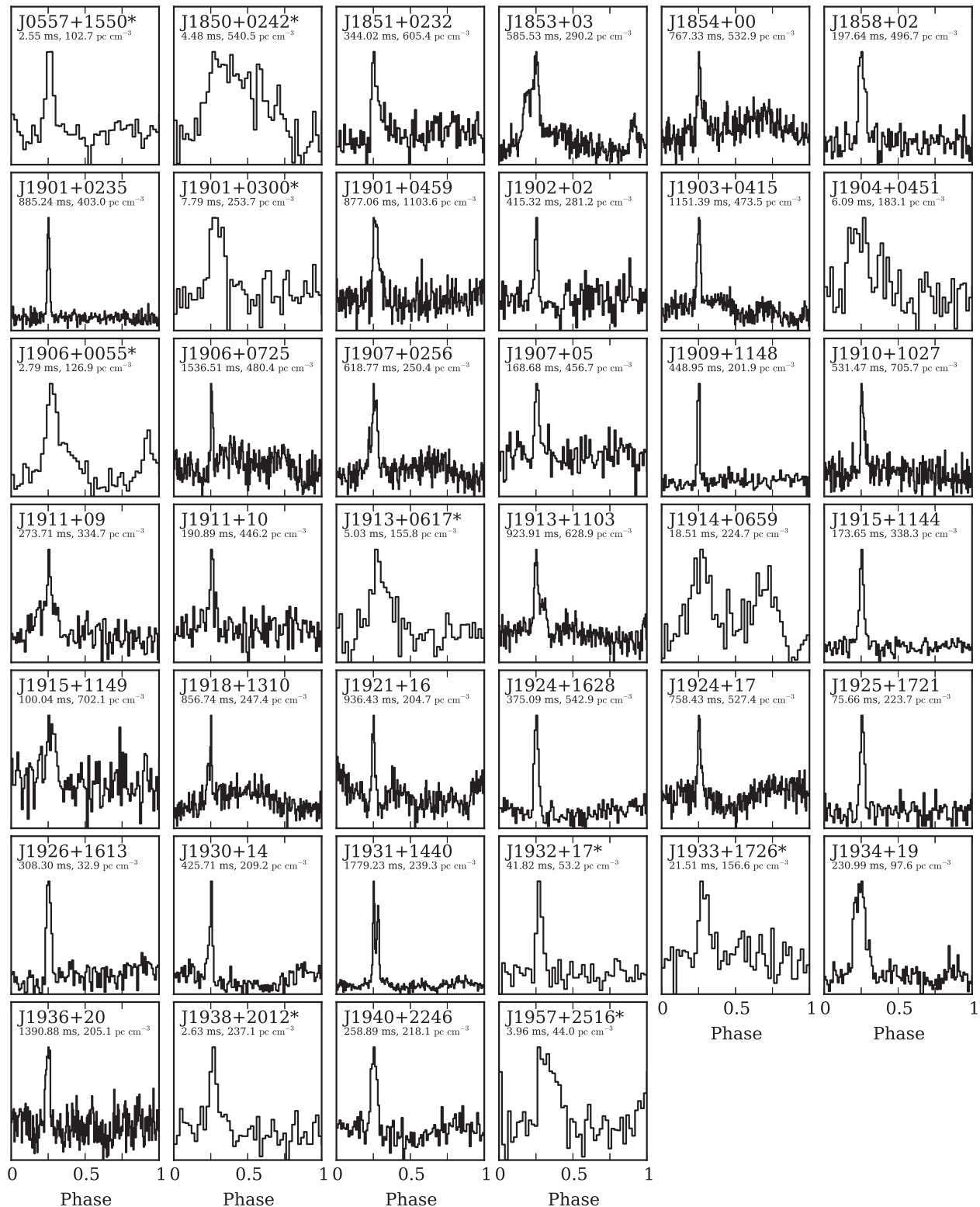
Figure 7. Pulse profiles at 1.4 GHz from the discovery observations of the 40 pulsars discovered with the PRESTO-based PALFA pipeline in Mock spectrometer data. The name of each pulsar is included above each profile along with the period, and dispersion measure. The names of binary pulsars are indicated with an asterisk (*). The number of bins across the profile is what was used by the pipeline, and is larger for longer period pulsars. These profiles also include intra-channel DM smearing, which is most significant for high-DM, short-period pulsars. The baselines of several profiles, predominantly of the long-period pulsars, show broad features due to interference and red noise in the data (for example, PSRs J1854+00, J1921+16, and J1924+17). The discovery profiles contaminated with RFI and red noise are shown here to highlight the ability of the PALFA pipeline to identify pulsars despite these conditions. Pulsars with truncated names do not yet have positions determined from timing campaigns.
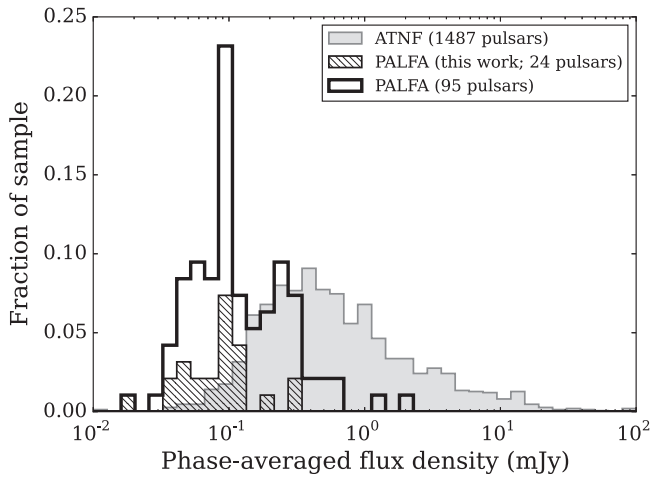
Figure 8. Distribution of phase-averaged flux densities of pulsars discovered in the PALFA survey, and the distribution of 1400 MHz phase-averaged flux densities from the ATNF pulsar catalog of all non-PALFA, non-globular cluster discoveries. The sub-set of PALFA pulsars featured in this work is highlighted. Only PALFA-discovered pulsars with timing positions are included.

The gain was scaled according to the angular offset of the pulsar from the beam center, θ, assuming an Airy disk beam pattern[38] with FWHM = 3′35 (Cordes et al. 2006), as well as the dependence on the zenith angle, ZA. The gain also took into account the ALFA beam with which the pulsar was detected. We scaled the gain of the outer 6 beams to be 79% of the gain of the central beam (Cordes et al. 2006).

Sky temperatures were scaled from the Haslam et al. (1982) 408 MHz survey to 1400 MHz using a spectral index of -2.76 for the Galactic synchrotron emission (Platania et al. 1998). The sky temperatures also include the 2.73 K cosmic microwave background.

The resulting phase-averaged flux density estimates (i.e., the integrated flux of the pulse divided by the pulse period) of the PALFA pulsars discovered with our pipeline range from 16 to 280 μJy (see Table 5), making them among the weakest detected pulsars in the Galactic field, along with other PALFA-discovered pulsars (see Figure 8).

4.2. Re-detections of Known Pulsars

In total, 83 pulsars for which 1400 MHz phase-averaged flux densities, S_{1400}, are reported in the ATNF catalog were detected with the Mock spectrometers in 268 different PALFA observations (i.e., some known pulsars were re-detected multiple times).

To confirm that our observing set-up is as sensitive as expected, we estimate the $(S/N)_T$ at which our pipeline should blindly re-detect known pulsars in our observations and compare with the $(S/N)_T$ measured from the profile of the corresponding candidate. The expected $(S/N)_T$ values were estimated by inverting Equation (3) to solve for the signal-to-noise ratio using S_{1400} from the ATNF catalog. As in Section 4.1 the telescope gain is modeled as an Airy disk with FWHM = 3′35.

---

[38] The FWHM of the ALFA beams varies by only ∼5% over the ZA range of the telescope. Also, FWHM of all 7 beams are largely consistent with each other. Thus, we use a fixed FWHM for all beams and all ZA.
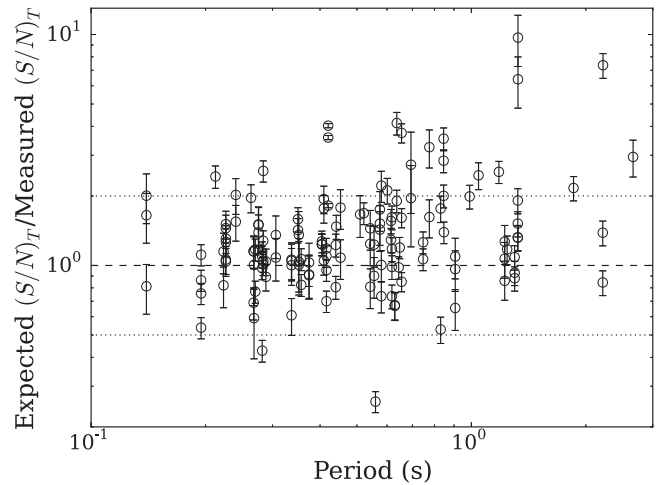

Figure 9. Ratio of expected and measured $(S/N)_T$ as a function of pulsar period. Expected $(S/N)_T$ values are calculated using the radiometer equation and measured flux densities at 1400 MHz from the ATNF catalog. Measured $(S/N)_T$ values are computed from detections of known pulsars in PALFA observations. The increased scatter and bias toward higher S/N ratios of longer-period pulsars are consistent with reduced sensitivity to these pulses due to red noise (see Section 5.4 and Figure 11). Known pulsars without reported flux densities and uncertainties are excluded, as are pulsars that have reported flux densities consistent with 0 mJy. Also excluded from the plot are 15 known pulsars with published flux densities that were detected in observations pointed more than 3′ from the position of the pulsar. This is because the actual beam pattern differs considerably from the theoretical Airy disk beam pattern beyond ∼3′, making it difficult to reliably estimate the expected $(S/N)_T$. The dashed line indicates equality of the expected and measured $(S/N)_T$ values, and the dotted lines are at a factor of two above and below equality.

By comparing expected and measured S/N against pulsar spin period we find that longer-period pulsars show an increase scatter in $(S/N)_T$ ratio as well as a bias toward larger ratios (see Figure 9). This is consistent with the reduced sensitivity to long-period pulsars due to red noise we find from our sensitivity analysis using synthetic pulsar signals (see Section 5).

In addition to the 83 known pulsars with published S_{1400} detected with the PALFA PRESTO pipeline, there are 50 more that do not have values for S_{1400} listed in the ATNF catalog. The complete list of 128 previously discovered pulsars blindly re-detected by the PALFA PRESTO pipeline is in Table 6.

4.3. Known Pulsars Missed

In addition to the 268 detections of 128 separate known pulsars mentioned in Section 4.2, there were 7 instances in which a known pulsar was not detected by the search pipeline, despite being detected when subsequently folding the search data with the most recently published ephemeris. In all cases the data were badly affected by RFI; there are strong signals within one Fourier bin of the pulsar period. Furthermore, these are long-period pulsars, which are more difficult to detect than expected due to red noise in the data. It is therefore not entirely surprising that these observations did not result in detections. A thorough analysis of the effects of RFI and red noise on the sensitivity to long period pulsars is therefore crucial, and forms the discussion of the following section.

5. ASSESSING THE SURVEY SENSITIVITY

The sensitivity of pulsar observations is typically estimated using the radiometer equation (Equation (3)). In principle, the

Table 6
Known Pulsars Re-detected in Mock Spectrometer Data with the PRESTO Pipeline

Name	Period (ms)	DM (pc cm^{-3})	ATNF S_{1400} (mJy)	Measured S/N	Measured S_{1400} (mJy)
B1848+04	284.70	115.5	0.66(8)	36.9	⋯
B1849+00	2180.20	787.0	2.2(2)	64.1	⋯
B1853+01	267.44	96.7	0.19(3)	99.7	0.323
B1854+00	356.93	82.4	0.9(1)	267.9	1.048
B1855+02	415.82	506.8	1.6(2)	470.2	2.288
B1859+01	288.22	105.4	0.38(5)	74.7	0.531
B1859+03	655.45	402.1	4.2(4)	1061.3	3.498
B1859+07	644.00	252.8	0.9(1)	339.1	1.830
B1900+01	729.30	245.2	5.5(6)	106.5	⋯
B1900+05	746.58	177.5	1.2(1)	283.2	1.228
B1900+06	673.50	502.9	1.1(1)	21.5	⋯
B1901+10	1856.57	135.0	0.58(7)	212.1	0.568
B1903+07	648.04	245.3	1.8(2)	91.2	1.892
B1904+06	267.28	472.8	1.7(2)	33.9	⋯
B1906+09	830.27	249.8	0.23(3)	17.7	0.127
B1907+02	989.83	171.7	0.63(7)	37.7	⋯
B1907+10	283.64	150.0	1.9(2)	365.2	2.591
B1907+12	1441.74	258.6	0.28(4)	28.2	0.196
B1910+10	409.35	147.0	0.22(3)	47.1	0.196
B1911+09	1241.96	157.0	0.14(2)	18.9	0.228
B1911+11	601.00	100.0	0.55(7)	85.4	0.301
B1911+13	521.47	145.1	1.2(1)	85.5	1.221
B1913+10	404.55	241.7	1.30(14)	416.8	0.905
B1913+105	628.97	387.2	0.22(3)	46.2	0.507
B1913+167	1616.23	62.6	⋯	16.1	⋯
B1914+09	270.25	61.0	0.9(1)	298.6	0.721
B1914+13	281.84	237.0	1.2(1)	616.7	2.043
B1915+13	194.63	94.5	1.9(2)	1453.2	4.477
B1916+14	1181.02	27.2	1.0(1)	14.3	0.362
B1919+14	618.18	91.6	0.68(8)	217.6	1.060
B1921+17	547.21	142.5	⋯	126.6	0.408
B1924+14	1324.92	211.4	0.48(6)	126.6	0.860
B1924+16	579.82	176.9	1.3(2)	179.1	0.735
B1925+18	482.77	254.0	⋯	156.0	0.441
B1925+188	298.31	99.0	⋯	77.3	0.385
B1929+15	314.36	140.0	⋯	69.4	0.360
B1929+20	268.22	211.2	1.2(4)	457.9	1.099
B1933+16	358.74	158.5	42(6)	73.0	⋯
B1933+17	654.41	214.6	⋯	62.8	0.176
B1937+21	1.56	71.0	13(5)	349.1	12.572
B1937+24	645.30	142.9	⋯	39.4	⋯
B1944+22	1334.45	140.0	⋯	55.0	0.173
B2002+31	2111.26	234.8	1.8(1)	68.2	⋯
J0621+1002	28.85	36.6	1.9(3)	11.4	⋯
J0625+10	498.40	78.0	⋯	14.5	0.086
J0631+1036	287.80	125.4	⋯	175.3	0.941
J1829+0000	199.15	114.0	⋯	52.4	0.370
J1843−0000	880.33	101.5	2.9(3)	38.5	⋯
J1844+00	460.50	345.5	8.6(9)	1226.8	4.616
J1849+0127	542.16	207.3	0.46(9)	143.2	0.444
J1849+0409	761.19	56.1	⋯	29.0	0.312
J1851+0118	906.98	418.0	0.10(2)	27.9	0.118
J1852+0305	1326.15	320.0	0.8(2)	37.7	0.214
J1853+0056	275.58	180.9	0.21(4)	55.3	0.281
J1853+0545	126.40	198.7	1.6(1.7)	5.3	⋯
J1854+0317	1366.45	404.0	0.12(1)	34.9	0.153
J1855+0307	845.35	402.5	1.0(1)	129.7	0.393
J1855+0422	1678.11	438.0	0.45(9)	104.0	0.245
J1856+0102	620.22	554.0	0.4(1)	66.3	0.195
J1856+0404	420.25	341.3	0.48(1)	40.4	0.276
J1857+0143	139.76	249.0	0.7(2)	37.2	0.486
J1857+0210	630.98	783.0	0.30(6)	40.2	0.236
J1857+0526	349.95	466.4	0.66(8)	145.5	0.645

Table 6
(Continued)

Name	Period (ms)	DM (pc cm^{-3})	ATNF S_{1400} (mJy)	Measured S/N	Measured S_{1400} (mJy)
J1858+0215	745.83	702.0	0.22(4)	42.8	0.280
J1859+00	559.63	420.0	4.8(5)	581.9	24.461
J1859+0601	1044.31	276.0	0.30(4)	15.9	0.126
J1900+0227	374.26	201.1	0.33(7)	111.6	0.414
J1901+00	777.66	345.5	0.35(4)	32.4	⋯
J1901+0254	1299.69	185.0	0.58(7)	102.1	0.911
J1901+0320	636.58	393.0	0.9(1)	67.3	0.301
J1901+0355	554.76	547.0	0.15(3)	40.9	0.185
J1901+0413	2663.08	352.0	1.1(2)	161.9	0.521
J1901+0435	690.58	1042.6	⋯	106.9	4.244
J1901+0510	614.76	429.0	0.66(8)	47.6	0.498
J1902+0248	1223.78	272.0	0.17(3)	60.6	0.169
J1903+0601	374.12	388.0	0.26(4)	9.7	⋯
J1904+0412	71.09	185.9	0.23(5)	68.4	0.271
J1904+0800	263.34	438.8	0.36(5)	11.2	0.285
J1905+0600	441.21	730.1	0.42(5)	85.6	0.401
J1905+0616	989.71	256.1	0.51(6)	43.5	0.236
J1906+0912	775.34	265.0	0.32(6)	34.0	0.149
J1907+0249	351.88	261.0	0.5(1)	124.3	0.478
J1907+0345	240.15	311.7	0.17(3)	21.5	0.133
J1907+0534	1138.40	524.0	0.36(7)	24.6	0.096
J1907+0731	363.68	239.8	0.35(4)	68.8	0.571
J1907+0740	574.70	332.0	0.41(8)	121.4	0.327
J1907+0918	226.11	357.9	0.29(4)	133.4	0.263
J1907+1149	1420.16	202.8	⋯	30.4	0.156
J1908+0457	846.79	360.0	0.9(1)	274.4	0.958
J1908+0500	291.02	201.4	0.79(9)	48.5	⋯
J1908+0734	212.35	11.1	0.54(6)	36.0	0.205
J1908+0839	185.40	512.1	0.49(1)	114.4	0.403
J1908+0909	336.55	467.5	0.22(4)	110.7	0.340
J1909+0616	755.99	352.0	0.33(7)	10.3	⋯
J1909+0912	222.95	421.5	0.35(7)	125.8	0.533
J1910+0534	452.87	484.0	0.41(8)	62.4	0.444
J1910+0714	2712.42	124.1	0.36(5)	137.3	0.287
J1910+0728	325.42	283.7	0.8(1)	189.8	0.887
J1910+1256	4.98	38.1	0.5(1)	139.7	0.497
J1913+0832	134.41	355.2	0.6(1)	187.9	0.999
J1913+0904	163.25	95.3	⋯	96.7	0.224
J1913+1000	837.15	422.0	0.53(6)	28.8	0.522
J1913+1011	35.91	178.8	0.5(1)	111.0	0.434
J1913+1145	306.07	637.0	0.43(9)	126.5	0.403
J1913+1330	923.39	175.6	⋯	213.6	⋯
J1914+0631	693.81	58.0	0.3(1)	36.9	0.140
J1915+0738	1542.70	39.0	0.34(4)	109.1	0.254
J1915+0752	2058.31	105.3	0.21(3)	18.2	0.238
J1915+0838	342.78	358.0	0.29(4)	12.3	⋯
J1915+1410	297.49	273.7	⋯	11.6	0.134
J1916+0748	541.75	304.0	2.8(3)	66.8	⋯
J1916+0844	440.00	339.4	0.44(5)	89.9	0.526
J1916+0852	2182.75	295.0	0.13(2)	36.6	0.148
J1920+1040	2215.80	304.0	0.57(7)	24.5	0.092
J1920+1110	509.89	182.0	0.39(8)	22.9	0.288
J1921+1544	143.58	385.0	⋯	65.5	0.211
J1922+1733	236.17	238.0	⋯	435.6	1.157
J1924+1639	158.04	208.0	⋯	73.6	0.207
J1926+2016	299.07	247.0	⋯	12.0	0.122
J1928+1923	817.33	476.0	⋯	221.7	0.639
J1929+1955	257.83	281.0	⋯	25.1	0.421
J1930+17	1609.69	201.0	⋯	30.9	⋯
J1931+1952	501.12	441.0	⋯	71.9	0.126
J1935+2025	80.12	182.0	⋯	79.6	0.527
J1936+21	642.93	264.0	⋯	13.6	⋯
J1938+2213	166.12	91.0	⋯	20.4	⋯

Table 6
(Continued)

Name	Period (ms)	DM (pc cm^{-3})	ATNF S_{1400} (mJy)	Measured S/N	Measured S_{1400} (mJy)
J1946+2611	435.06	165.0	⋯	232.0	0.697
J1957+2831	307.68	139.0	1.0(2)	34.4	⋯

Note. Values for period, DM, and "ATNF S_{1400}" are taken from the ATNF Catalogue (Manchester et al. 2005).

Table 7
Synthetic Pulsar Signal Parameters

Parameter	Possible Values						
	0.766	1.102	2.218	5.218	10.870	18.505	26.965
Period, ms	61.631	126.175	286.555	533.320	850.158	1657.496	2643.410
	3927.013	5580.899	10964.532	⋯	⋯	⋯	⋯
DM, pc cm^{-3}	10	40	150	325	400	600	1000
FWHM, % Phase	1.5	2.6	5.9	11.9	24.3	⋯	⋯

effects of DM, period, and pulse width on sensitivity are adequately described by the radiometer equation. The expression derived by Cordes & Chernoff (1997, see their Appendix A), includes a more complete description of pulse shape and the effect of DM, which causes distortions of the pulse profile. However, neither of these equations includes the effect of RFI. In this section, we describe a prescription for accurately modeling the sensitivity of pulsar search observations including the effect of RFI, as well as its dependence on period, DM, and pulse width.

To estimate the survey sensitivity we injected synthetic pulsar signals into actual survey data, and attempted to recover the period and DM of the input signal using our pipeline. By using synthetic signals we can also better determine the selection effects imposed by our pipeline.

5.1. Constructing a Synthetic Pulsar Signal

For this work, a simple synthetic pulsar signal was constructed for a given combination of period, DM, phase-averaged flux density, and profile shape. Once the relevant parameters were chosen (see Section 5.3 and Table 7), a two-dimensional pulse profile (intensity versus spin phase and observing frequency) was generated.

The pulse profile of each frequency channel was smeared by convolving with a box-car whose phase width corresponded to the dispersion delay within the channel, as well as scattered by convolving with a one-sided exponential function with a characteristic phase width corresponding to the pulse broadening timescale. We determined the scattering timescale using version of Equation (1) from Cordes et al. (2002). Care was taken to conserve the area under the profile during the convolutions. The scaling factor applied to the synthetic signals was determined by flux-calibrating the PALFA observing system (see Section 5.2).

5.2. Calibration

On 2013 December 21, we observed the radio galaxy 3C 138 in order to calibrate the central beam of ALFA. Three observations using the standard survey set-up described in Section 2 were conducted, but with 5 minute integrations, and with the calibration diode being pulsed on and off at 40 Hz. The on-source scan of 3C 138 was preceded by an off-source

scan 0°.5 to the north of 3C 138 and followed by a similar off-source scan 0°.5 to the south.

The calibration observation data were converted to 4-bit samples, and the Mock spectrometer sub-bands were combined (see Section 3.2). The data were folded at the modulation frequency of the calibrator diode using fold_psrfits of psrfits_utils. Next, the on-cal and off-cal levels in the on-source and off-source observations were used to relate the flux density of the calibration diode with the cataloged flux density of 3C 138 (for details, see e.g., Lorimer & Kramer 2004, page 176). The result is the flux density of the calibration diode as a function of observing frequency. In practice, this was done using fluxcal of psrchive.[39]

The per-channel scaling factors between flux density and the observation data units were determined by applying the calibration solution along with the calibration diode signal. This procedure determines the absolute level of the injected signal corresponding to a target phase-averaged flux density, as well as the shape of the bandpass, which was retained thanks to the PSRFITS scales and offsets (see Section 2).

5.3. Injection Trials

Artificial pulsar signals were injected into the data by summing the two-dimensional, smeared, scattered, and scaled synthetic pulse profile with the data at regular intervals corresponding to the period of the synthetic pulsar. The scaling was determined using the calibration procedure described in Section 5.2. The resulting data file, including the injected signal, was written out with 32 bit floating-point samples in SIGPROC "filterbank" format[40] for simplicity, without re-quantizing the data. Neither using 32-bit floating-point samples nor filterbank format data should significantly influence the results.

Many synthetic signals with a broad range of parameters were required to build a comprehensive picture of the survey sensitivity (see Table 7). In total, 17 periods were selected between 0.77 ms and 11 s along with six DMs ranging from 10 to 1000 pc cm^{-3}. In all cases, the profile of the synthetic signal was chosen to have a single centered von Mises component

---

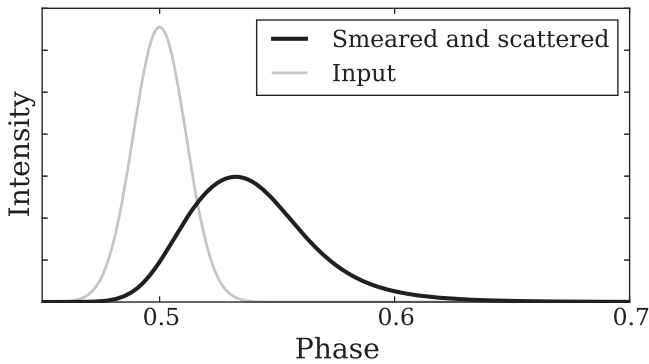[39] http://psrchive.sourceforge.net/
[40] http://sigproc.sourceforge.net/

Figure 10. Profile of a synthetic $P = 5$ ms pulsar consisting of a single von Mises component with FWHM = 2.6% (gray), and the same profile broadened according to DM = 250 pc cm^{-3}. The broadening is caused by dispersive smearing within each channel and scattering according to Equation (1). Note that the plot is zoomed into the region: $0.45 < \phi < 0.7$.

with a FWHM selected from 5 possible values between $\sim$1.5% and $\sim$24% of the period. The example profile in Figure 10 shows the case where FWHM = 2.6%. The synthetic signals were injected into 12 different observations to determine the survey sensitivity in a variety of RFI conditions. All 12 observations used in this analysis are from late 2013 and from the central beam of ALFA. Although the gains of the outer beams are lower than that of the central beam, the response of the observing system and pulsar search pipeline to RFI and red noise derived for the central beam should also apply to the outer beams.

The total number of combinations of synthetic signals and observations is >7000. Multiple trials, each with a different amplitude, were constructed, injected, and searched to determine the sensitivity limit at each point in (period, DM, pulse FWHM) phase-space. To reduce the computational burden, not all possible combinations of parameters were used. In particular, only the profile with FWHM $\sim$2.6% was injected into all 12 observations. The remaining four profiles shapes were only injected into a single observation. This still permits the determination of the dependence of the minimum detectable flux density, S_{min}, on pulse width.

In addition to injecting synthetic pulsars into the 12 survey observations, we also conducted a series of trials where we injected the FWHM $\sim$2.6% signal into 5 independently simulated observations consisting of pure white noise.

5.4. Realistic Survey Sensitivity

It is well known (Dewey et al. 1985) that the S_{min} of a pulsar depends on the intrinsic width of its profile, as well as the DM, because dispersive smearing and scattering broaden the profile. It is also reasonable to expect a reduction of sensitivity due to RFI and red noise, even with the red noise suppression algorithms employed (see Section 3.4.4). By recovering injected signals using the pipeline described in Section 3, we have determined the true sensitivity of the PALFA survey, and its dependence on spin period and DM (see Figure 11). We found the commonly used version of the radiometer equation (Equation (3); Dewey et al. 1985) overestimates the survey sensitivity to long-period pulsars. For example, for $P = 0.1$–2.0 s pulsars with DM >150 pc cm^{-3} (the majority of the pulsars we expect to find with PALFA), the degradation in sensitivity compared with the ideal case is a factor of $\sim$1.1–2.

We have also confirmed the claim by Cordes & Chernoff (1997) that the Dewey et al. (1985) radiometer equation underestimates the sensitivity to high-DM MSPs, by not correctly modeling the distortion of the profile due to smearing and scattering. The more accurate variant of the radiometer equation from Cordes & Chernoff (1997) better matches our measured sensitivity curves in the MSP regime, thanks to its inclusion of the profile shape and distortions. However, the degraded sensitivity we find at long periods is still not properly modeled with these adjustments.

Red noise present in pulsar search data due to RFI, receiver gain fluctuations, and opacity variations of the atmosphere makes it difficult to detect long-period radio pulsars. Our analysis has shown that for the PALFA survey, at low DMs, the reduction in sensitivity already affects pulsars with periods of $\sim$100 ms. Fortunately, the effect is slightly less significant for pulsars with higher DMs. This is evident in Figure 11.

We have parameterized the sensitivity curves by fitting $\log S_{min}$ versus DM with a cubic function and modeling how these curves depend on period. To estimate S_{min} at an arbitrary profile width, we first estimate S_{min} at each of the five trial widths, then fit a quadratic function in $\log S_{min}$ versus width, and use the parameters of the fit to calculate S_{min} at the desired width. This empirical scheme provides reliable estimates of S_{min} within the intervals used for trial values of period, DM, and width. Sensitivity maps for each of the five profile widths used are shown in Figure 12.

6. POPULATION SYNTHESIS ANALYSIS

We have used the sensitivity curves determined above (see Section 5.4) to re-evaluate the expected yield of the PALFA survey by performing a population synthesis analysis with `PsrPopPy`[41] (Bates et al. 2014).

Galactic populations of non-recycled pulsars were simulated using the radial distribution from Lorimer et al. (2006a) and a Gaussian distribution of heights above/below the plane with a scale height of 330 pc. The pulsar periods were described by a log-normal distribution with $\langle \log P \rangle = 2.7$ and $\sigma_{\log P} = -0.34$ (Lorimer et al. 2006a). The pulse-width-to-period relationship was also taken from Lorimer et al. (2006a). We used a log-normal luminosity distribution described by the best-fit parameters found by Faucher-Giguère & Kaspi (2006), $\langle \log L \rangle = -1.1$ and $\sigma_{\log L} = 0.9$.

We created 5000 simulated pulsar populations, each containing enough pulsars such that a simulated version of the Parkes multi-beam surveys detected 1038 pulsars, the number of non-recycled pulsars detected by the actual surveys. We then compared the pulsars in each of these populations against a list of PALFA observations,[42] and estimated their significance using the radiometer equation. Pulsars with $(S/N)_{expect} > 11.3$ were considered "detectable."[43] Next, we compared the flux-density for each "detectable" pulsar against the parameterized PALFA sensitivity curves to determine if the pulsar also has a

---

[41] https://github.com/samb8s/PsrPopPy
[42] For each observation we used the sky position, integration time, zenith angle, and beam number. We used the model of gain and system temperature dependence on zenith angle provided by the observatory. We assumed the six outer beams have a gain of $\sim$80% of the central beam, consistent with the gains reported by Cordes et al. (2006).
[43] The value of $(S/N)_{expect}$ was chosen such that the minimum detectable flux density coincided with the measured sensitivity curves for a duty cycle of 2.6%.
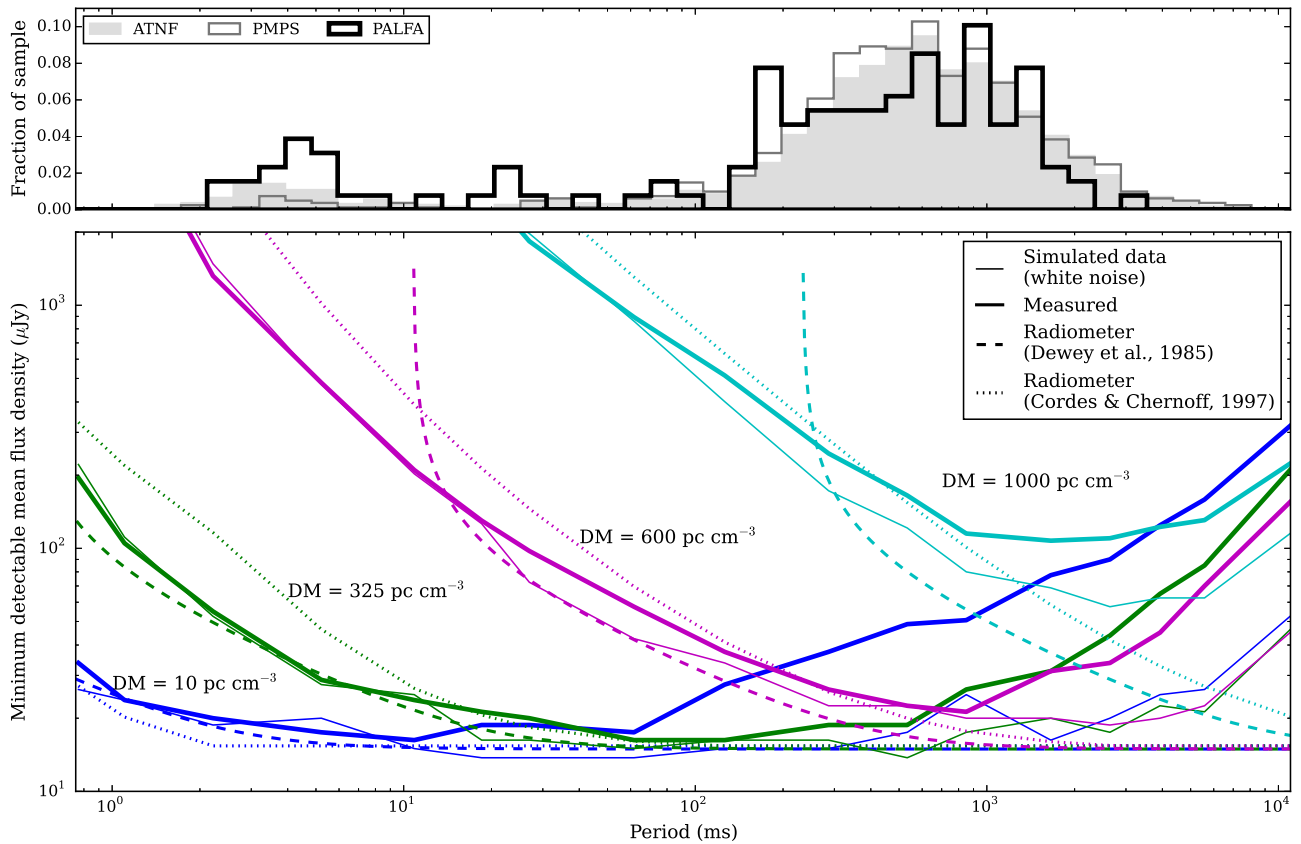
Figure 11. *Top*—Period distribution of all Galactic radio pulsars, excluding RRATs, listed in the ATNF catalog. Pulsars discovered in the Parkes Multibeam Pulsar Survey of the Galactic Plane (PMPS) are highlighted, as are as those found in PALFA. *Bottom*—Minimum detectable phase-averaged flux density curves for the PALFA survey as measured using synthetic pulsar signals with FWHM = 2.6% (thick solid lines). Only four of the seven trial DM values are shown here for clarity; these are DM = 10 pc cm^{-3} (dark blue), 325 pc cm^{-3} (green), 600 pc cm^{-3} (purple), and 1000 pc cm^{-3} (light blue). The omitted trials (DM = 40, 150, and 400 pc cm^{-3}) exhibit similar behavior. The majority of the reduction in sensitivity at long periods is due to RFI and red noise in the data. This is especially clear when comparing against the pipeline sensitivity we determined by injecting synthetic pulsar signals into simulated purely Gaussian distributed noise (thin lines). Furthermore, we see clear discrepancies when comparing the measured curves with the analogous sensitivity limits derived with the commonly used radiometer equation (Dewey et al. 1985) (dashed lines). Sensitivity to long-period pulsars is overestimated, and sensitivity to MSPs is underestimated. However, the formulation of the radiometer equation by Cordes & Chernoff (1997, dotted lines) is more complete—albeit less frequently used—and better models the sensitivity in the short-period regime. See Section 5.4 for details.

sufficiently large flux density to lie above the measured sensitivity curves. For each pulsar, the measured sensitivity curves are shifted according to the zenith angle of the observation, the gain of the beam used, the sky temperature and the angular offset between the pulsar position and the beam center.

We found 33 ± 3% of the simulated pulsars having fluxes above the theoretical sensitivity threshold derived from the radiometer equation (Equation (3)) are not sufficiently bright to also be "detected" by our measured sensitivity limits for the PALFA survey (e.g., Figure 12) due to the residual effect of red noise and RFI following the extensive mitigation procedures described in Section 3.4. The median period of the pulsars missed is $P_{\rm miss} \simeq 585$ ms, which is considerably longer than the median period of the potentially detectable pulsars brighter than the radiometer-equation-based threshold, $P_{\rm det.} \simeq 440$ ms (see Figure 13).

Our 5000 realizations of simulated Galactic pulsar populations, adjusted for the reduced sensitivity to long-period pulsars, suggest 224 ± 16 un-recycled pulsars should be detected in PALFA Mock spectrometer observations, given the current processed pointing list. As of 2015 January, 241 un-recycled pulsars have been discovered/detected in PALFA observations with the Mock spectrometers.

The number of un-recycled pulsar detections predicted for the PALFA survey by Swiggum et al. (2014) is an overestimate for two reasons. First, their analysis used a threshold S/N = 9. Given the observing parameters assumed, a more appropriate threshold of S/N = 11.3 should have been used to correspond to the minimum detectable flux density we find ($S_{\rm min} = 0.015$ mJy). Second, the analysis by Swiggum et al. (2014) did not include the effect of red noise, which we have shown reduces the number of pulsars expected to be found in the PALFA survey by 33%.

7. DISCUSSION

The detailed sensitivity analysis of Section 5.4 confirms that, on average, the PALFA survey is as sensitive to MSPs and mildly recycled pulsars as expected from the radiometer equation. However, the survey is less sensitive to long-period pulsars than predicted. The degradation in sensitivity is between 10% and a factor of 2 for the majority of pulsars we expect to find in the PALFA survey (spin periods between 0.1 s and 2 s and DM > 150 pc cm^{-3}), and up to a factor of ∼10 in the worst case (DM < 100 pc cm^{-3} and P > 2 s; this fortunately corresponds to a parameter space that contains far
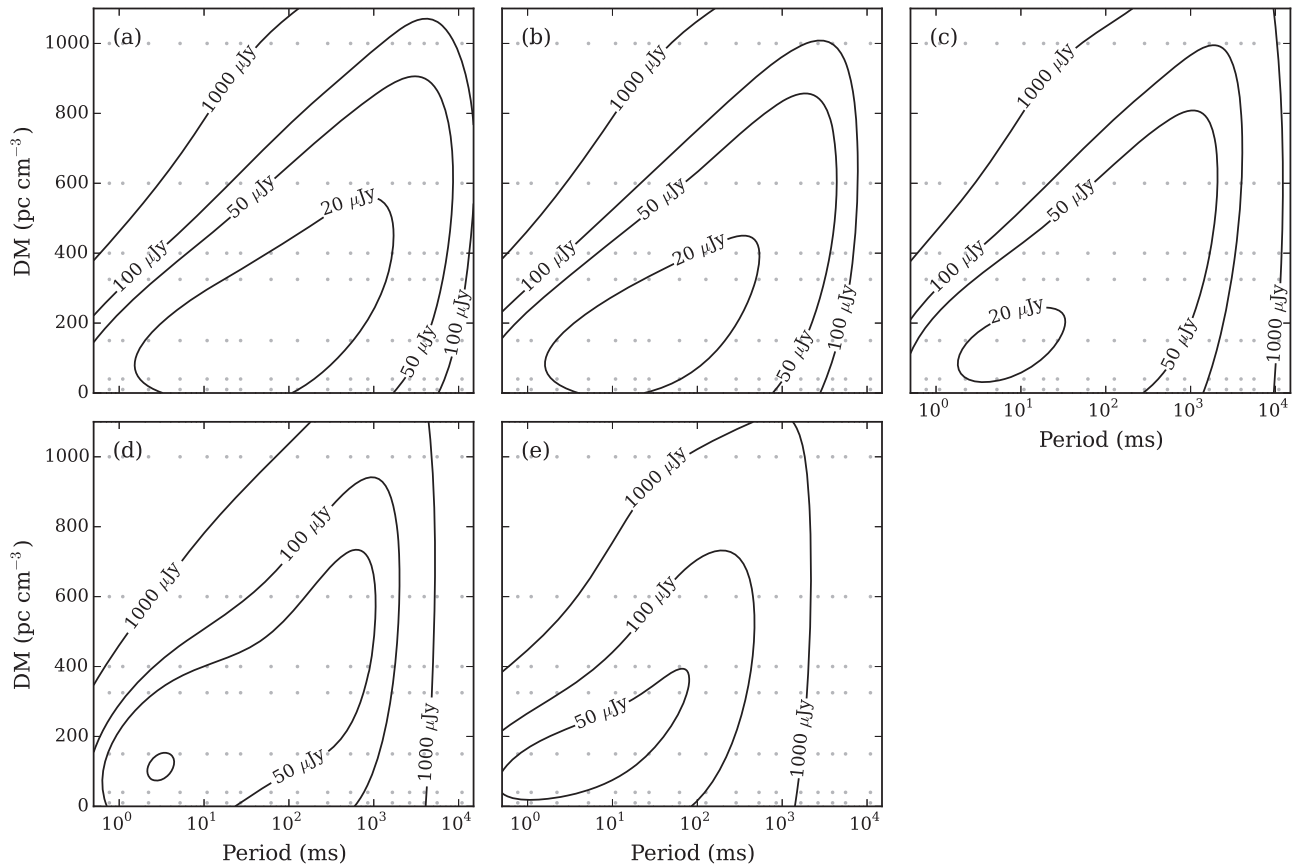
Figure 12. PALFA survey sensitivity as a function of DM and spin period. The maps are determined using synthetic pulsar signals injected into observations and recovered using the pipeline. Contours correspond to minimum detectable phase-averaged flux densities of 20, 50, 100, 1000 μJy. The five panels (a)–(e) correspond to profile FWHMs of 1.5%, 2.6%, 5.9%, 11.9%, 24.3%, respectively. In all cases, the profile consists of a single centered von Mises component (see Figure 10 for an example). The period, DM combinations used in the sensitivity analysis are shown with the small dots.

fewer expected pulsars). The reduction of sensitivity is mostly caused by red noise present in the observations (see Figure 11).

The empirical sensitivity curves we determined apply specifically to the PALFA survey, its observing set-up, and the search algorithms used. Because the effects of red noise on radio pulsar survey sensitivity have the potential to be significant, as in the case of PALFA, we strongly suggest measuring the impact of red noise on other surveys by performing similar analyses to what we described in Section 5. Also, future population analyses should include these measured effects of red noise rather than assuming the theoretical radiometer equation (e.g., Faucher-Giguère & Kaspi 2006; Lorimer et al. 2006a) when deriving spatial, spin, and luminosity distributions for the underlying Galactic population of pulsars.

What are the potential ramifications of reduced sensitivity to long-period pulsars being unaccounted for in population synthesis analyses? First, the existence of radio-loud pulsars beyond the "death line" is important to our understanding of the radio emission mechanism in pulsars. For example, the existence of the 8.5 s PSR J2144−3933 contradicted several existing emission theories (Young et al. 1999; Zhang et al. 2000). The existence of a larger population of slowly rotating pulsars, particularly the discovery of pulsars so slow that existing theories cannot explain their radio emission, would further constrain models.

It is also possible there is a larger population of highly magnetized rotation-powered pulsars and quiescent radio-loud

magnetars that have been missed by the lower than predicted sensitivity of pulsar surveys. Radio emission from three of the four known radio-loud magnetars was detected following high-energy radiative events (Camilo et al. 2006, 2007; Eatough et al. 2013; Shannon & Johnston 2013). However, the other radio-loud magnetar PSR J1622−4950 was discovered from its radio emission (Levin et al. 2010; Olausen & Kaspi 2014). There is no evidence that the turn-on of PSR J1622−4950 at radio wavelengths was preceded by a high-energy event. The possibility that radio emission from magnetars is not always accompanied by X-ray or γ-ray emission means it is crucial to understand the biases against finding such long-period pulsars. Characterizing, and hopefully uncovering a hidden population of radio-loud magnetars, as well as highly magnetized-rotation powered pulsars, will help clarify the relationship between these two classes of pulsars, as well as the influence of strong magnetic fields on emission properties (e.g., flux and spectral index variability).

It may be possible to address the reduced sensitivity to long-period pulsars by using algorithms that perform better in the presence of red noise, as well as algorithms that remove red noise without suppressing the pulsar signal.

Long-period pulsars may be found via their harmonics even if red noise obscures the signal in the Fourier domain at the fundamental frequency of the pulsar, or if the power of the fundamental is suppressed by the red noise removal algorithm. As a result, the total summed power of the pulsar signal will not include the power of the fundamental and possibly even low
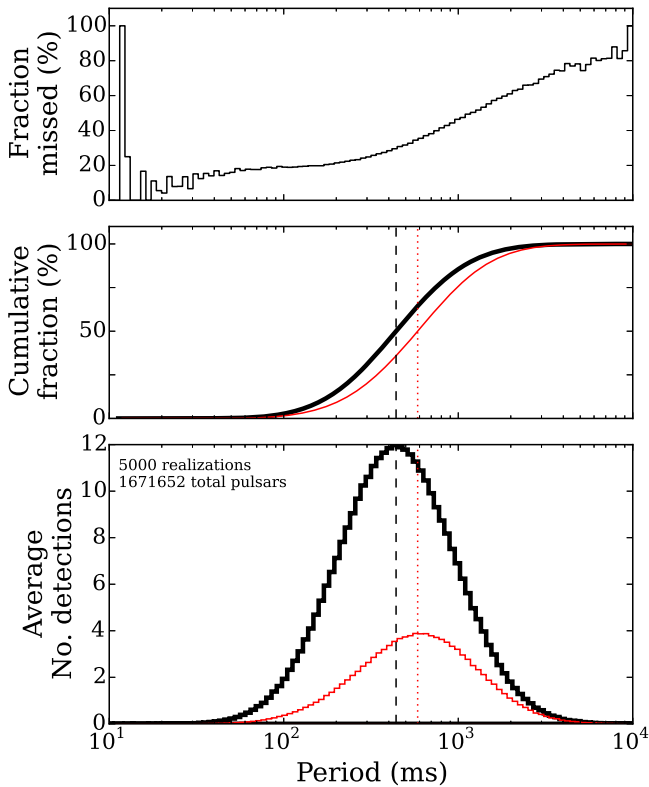
Figure 13. *Top*—Fraction of potentially detectable pulsars missed by PALFA due to red noise as a function of spin period, assuming the underlying pulsar population is accurately modeled by our input distributions (i.e., the distributions in Lorimer et al. 2006a, see Section 6). *Middle*—Cumulative fraction of simulated pulsars (thick black line), and pulsars missed (thin red line) as a function of pulse period. *Bottom*—Period distribution of potentially detectable simulated population of un-recycled pulsars averaged over 5000 realizations (thick black line) compared with the period distribution of pulsars expected to be missed due to red noise (thin red line). The median spin period of the potential detectable pulsars ($P \simeq 440$ ms) is shown by the dashed black line, and the median spin period ($P \simeq 585$ ms) of the missed pulsars is shown by the dotted red line.

harmonic frequencies, which can contain large amounts of power, especially in the case of pulsars with wide profiles. Furthermore, by not being based at the fundamental frequency of the pulsar, the total summed power will not include the power of slower, more significant harmonics in favor of weaker harmonics at higher frequencies. Despite the reduction in sensitivity several pulsars have been found in the PALFA survey thanks to their higher harmonic content.

One suggested method of improving sensitivity to long-period pulsars is by using the Fast-folding algorithm (FFA; see e.g., Lorimer & Kramer 2004, page 151; Kondratiev et al. 2009, and references therein). The periodograms produced by the FFA, a time-domain algorithm, are generated from computing a significance metric from pulse profiles. Thus, the broad profile features caused by red noise pose a problem for FFA-based searches. In short, the FFA is not immune to the degradation of sensitivity to long-period pulsars described above. However it does have the advantage of coherently summing *all* harmonics of a given period and greater period resolution than the DFT. These two factors should make the FFA slightly more sensitive to long-period pulsars, especially those with narrow profiles, than the Fourier Transform techniques described in Section 3.3.2, which is limited in the number of harmonics that can be summed (typically

incoherently; Kondratiev et al. 2009). The FFA has only been used sparingly in large-scale pulsar searches (e.g., Kondratiev et al. 2009). A more systematic investigation and application of the FFA is warranted.

Another algorithm that might have better performance in the presence of red noise is the single-pulse search technique described in Section 3.3.3. Single-pulse search algorithms are known to be more sensitive than standard FFT techniques to long-period pulsars in short observations (Deneva et al. 2009; Karako-Argaman et al. 2015). This is because of the natural variability of pulsar pulses and small number of pulses. Pulse-to-pulse variability was not included in the synthetic pulsar signals used in our sensitivity analysis and no single pulse searching was performed. It is likely that the sensitivity curves determined in this work are partially compensated by the single-pulse search techniques already in place, especially considering the recent suggestion that pulsars with $P > 200$ ms have a greater likelihood of being detected in single-pulse searches than faster pulsars (Karako-Argaman et al. 2015), at least in short integrations like the ones employed in PALFA observations. However, the extent of this compensation depends on the pulse-energy distributions of pulsars and the relative significances of their detections in periodicity and single-pulse searches.

8. CONCLUSIONS

We described the PRESTO-based PALFA pipeline, the primary data analysis pipeline used to search PALFA observations made with the Mock spectrometers. This pipeline has led to the discovery of 40 pulsars in periodicity searches and 5 RRATs, the re-detection of 60 pulsars previously discovered in the survey (using other pipelines), and the detection of 128 previously known pulsars. The PRESTO-based pipeline described here consists of several complementary search algorithms and RFI-mitigation strategies. The performance of the pipeline was determined by injecting synthetic pulses into actual survey observations and recovering the signals.

We have found that the PALFA survey is as sensitive to fast-spinning pulsars as expected by the theoretical radiometer equation. However, in the case of long-period pulsars, we have found that there is a reduction in the sensitivity due to RFI and red noise in the observations. The actual detection threshold for pulsars with $P > 4$ s at DM < 150 pc cm^{-3} is up to ~10 times higher than predicted by the theoretical radiometer equation. We have performed a population synthesis analysis using this empirical model of the survey sensitivity. Our analysis indicates that $33 \pm 3\%$ of pulsars, with predominantly long periods, are missed by PALFA, compared to expectations based on theoretical sensitivity curves derived using the radiometer equation.

The magnitude of the effect of red noise on the PALFA survey's sensitivity to long-period pulsars is surprising and should be taken into account in future population synthesis analyses. Furthermore, the effect of red noise on other radio pulsar surveys should be quantified in a similar manner and be included in population synthesis analyses to ensure the distributions determined for the underlying pulsar population are robust. The presence of more long-period pulsars could have implications on the location of the pulsar death line, the structure of pulsar magnetospheres and radio emission mechanism, as well as the relationship between canonical

pulsars, highly magnetized rotation-powered pulsars, radio-loud magnetars, and RRATs.

REFERENCES

Allen, B., Knispel, B., Cordes, J. M., et al. 2013, ApJ, 773, 91
Alpar, M. A., Cheng, A. F., Ruderman, M. A., & Shaham, J. 1982, Natur, 300, 728
Antoniadis, J., Freire, P. C. C., Wex, N., et al. 2013, Sci, 340, 448
Barr, E. D., Champion, D. J., Kramer, M., et al. 2013, MNRAS, 435, 2234
Bates, S. D., Lorimer, D. R., Rane, A., & Swiggum, J. 2014, MNRAS, 439, 2893
Bhat, N. D. R., Cordes, J. M., Camilo, F., Nice, D. J., & Lorimer, D. R. 2004, ApJ, 605, 759
Burke-Spolaor, S., Bailes, M., Ekers, R., Macquart, J.-P., & Crawford, F., III 2011, ApJ, 727, 18
Camilo, F., Ransom, S. M., Halpern, J. P., & Reynolds, J. 2007, ApJL, 666, L93
Camilo, F., Ransom, S. M., Halpern, J. P., et al. 2006, Natur, 442, 892
Champion, D. J., Ransom, S. M., Lazarus, P., et al. 2008, Sci, 320, 1309

Coenen, T., van Leeuwen, J., Hessels, J. W. T., et al. 2014, A&A, 570, A60
Cordes, J. M. 2002, in ASP Conf. Ser. 278, Single-Dish Radio Astronomy: Techniques and Applications, ed. S. Stanimirovic et al. (San Francisco, CA: ASP), 227
Cordes, J. M., & Chernoff, D. F. 1997, ApJ, 482, 971
Cordes, J. M., Freire, P. C. C., Lorimer, D. R., et al. 2006, ApJ, 637, 446
Cordes, J. M., & Lazio, T. J. W. 2002, arXiv:astro-ph/0207156
Cordes, J. M., & McLaughlin, M. A. 2003, ApJ, 596, 1142
Crawford, F., Stovall, K., Lyne, A. G., et al. 2012, ApJ, 757, 90
Demorest, P. B., Pennucci, T., Ransom, S. M., Roberts, M. S. E., & Hessels, J. W. T. 2010, Natur, 467, 1081
Deneva, J. S., Cordes, J. M., McLaughlin, M. A., et al. 2009, ApJ, 703, 2259
Deneva, J. S., Stovall, K., McLaughlin, M. A., et al. 2013, ApJ, 775, 51
Desvignes, G., Cognard, I., Champion, D., et al. 2013, in IAU Symp. 291, Neutron Stars and Pulsars: Challenges and Opportunities After 80 Years, ed. J. van Leeuwen (Paris: IAU), 375
Dewey, R. J., Taylor, J. H., Weisberg, J. M., & Stokes, G. H. 1985, ApJL, 294, L25
Dowd, A., Sisk, W., & Hagen, J. 2000, in ASP Conf. Ser. 202, IAU Coll. 177: Pulsar Astronomy—2000 and Beyond, ed. M. Kramer, N. Wex, & R. Wielebinski (San Francisco, CA: ASP), 275
Eatough, R. P., Falcke, H., Karuppusamy, R., et al. 2013, Natur, 501, 391
Eatough, R. P., Keane, E. F., & Lyne, A. G. 2009, MNRAS, 395, 410
Faucher-Giguère, C.-A., & Kaspi, V. M. 2006, ApJ, 643, 332
Hankins, T. H., Kern, J. S., Weatherall, J. C., & Eilek, J. A. 2003, Natur, 422, 141
Haslam, C. G. T., Salter, C. J., Stoffel, H., & Wilson, W. E. 1982, A&AS, 47, 1
Henning, P. A., Springob, C. M., Minchin, R. F., et al. 2010, AJ, 139, 2130
Hermsen, W., Hessels, J. W. T., Kuiper, L., et al. 2013, Sci, 339, 436
Hessels, J. W. T., Nice, D. J., Gaensler, B. M., et al. 2008, ApJL, 682, L41
Hessels, J. W. T., Ransom, S. M., Stairs, I. H., et al. 2006, Sci, 311, 1901
Hotan, A. W., van Straten, W., & Manchester, R. N. 2004, PASA, 21, 302
Karako-Argaman, C., Kaspi, V. M., Lynch, R. S., et al. 2015, ApJ, 809, 67
Keith, M. J., Jameson, A., van Straten, W., et al. 2010, MNRAS, 409, 619
Kiddle, C., Andrecut, M., Brazier, A., et al. 2011, in ASP Conf. Ser. 442, Astronomical Data Analysis Software and Systems XX, ed. I. N. Evans et al. (San Francisco, CA: ASP), 669
Kondratiev, V. I., McLaughlin, M. A., Lorimer, D. R., et al. 2009, ApJ, 702, 692
Kouwenhoven, M. L. A., & Voûte, J. L. L. 2001, A&A, 378, 700
Kramer, M., Lyne, A. G., O'Brien, J. T., Jordan, C. A., & Lorimer, D. R. 2006a, Sci, 312, 549
Kramer, M., Stairs, I. H., Manchester, R. N., et al. 2006b, Sci, 314, 97
Levin, L., Bailes, M., Bates, S., et al. 2010, ApJL, 721, L33
Liu, B., McIntyre, T., Terzian, Y., et al. 2013, AJ, 146, 80
Lorimer, D. R., Faulkner, A. J., Lyne, A. G., et al. 2006a, MNRAS, 372, 777
Lorimer, D. R., & Kramer, M. 2004, Handbook of Pulsar Astronomy, ed. R. Ellis et al. (Cambridge: Cambridge Univ. Press)
Lorimer, D. R., Stairs, I. H., Freire, P. C., et al. 2006b, ApJ, 640, 428
Lyne, A., Hobbs, G., Kramer, M., Stairs, I., & Stappers, B. 2010, Sci, 329, 408
Manchester, R. N., Hobbs, G. B., Teoh, A., & Hobbs, M. 2005, AJ, 129, 1993
Manchester, R. N., Lyne, A. G., Camilo, F., et al. 2001, MNRAS, 328, 17
Olausen, S. A., & Kaspi, V. M. 2014, ApJS, 212, 6
Petroff, E., Keane, E. F., Barr, E. D., et al. 2015, MNRAS, 451, 02165
Platania, P., Bensadoun, M., Bersanelli, M., et al. 1998, ApJ, 505, 473
Ransom, S. M. 2001, PhD thesis, Harvard Univ.
Ransom, S. M., Eikenberry, S. S., & Middleditch, J. 2002, AJ, 124, 1788
Scholz, P., Kaspi, V. M., Lyne, A. G., et al. 2015, ApJ, 800, 123
Shannon, R. M., & Johnston, S. 2013, MNRAS, 435, L29
Spitler, L. G. 2013, PhD thesis, Cornell Univ.
Spitler, L. G., Cordes, J. M., Hessels, J. W. T., et al. 2014, ApJ, 790, 101
Stovall, K. 2013, PhD thesis, The Univ. Texas
Stovall, K., Lynch, R. S., Ransom, S. M., et al. 2014, ApJ, 791, 67
Swiggum, J. K., Lorimer, D. R., McLaughlin, M. A., et al. 2014, ApJ, 787, 137
Thornton, D., Stappers, B., Bailes, M., et al. 2013, Sci, 341, 53
Young, M. D., Manchester, R. N., & Johnston, S. 1999, Natur, 400, 848
Zhang, B., Harding, A. K., & Muslimov, A. G. 2000, ApJL, 531, L135
Zhu, W. W., Berndsen, A., Madsen, E. C., et al. 2014, ApJ, 781, 117